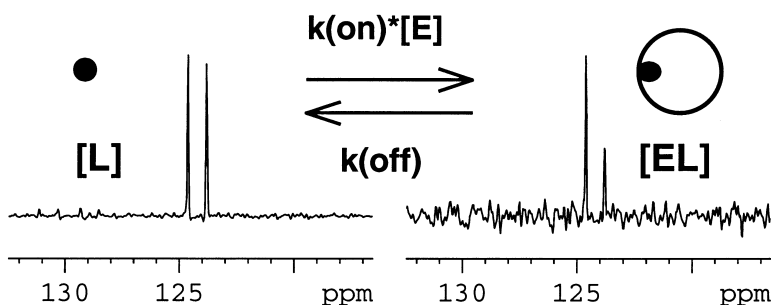Article

New Probes of Ligand Flexibility in Drug Design: Transferred C CSA−Dipolar Cross-Correlated Relaxation at Natural Abundance

Jeffrey W. Peng

More About This Article

Additional resources and features associated with this article are available within the HTML version:

- Supporting Information
- Links to the 3 articles that cite this article, as of the time of this article download
- Access to high resolution figures
- Links to articles and content related to this article
- Copyright permission to reproduce figures and/or text from this article

View the Full Text HTML

New Probes of Ligand Flexibility in Drug Design: Transferred ^{13}C CSA–Dipolar Cross-Correlated Relaxation at Natural Abundance

Jeffrey W. Peng*,†

Contribution from Vertex Pharmaceuticals, Inc., 130 Waverly Street, Cambridge, Massachusetts 02139

Received March 7, 2003; Revised Manuscript Received May 7, 2003; E-mail: Jeffrey.W.Peng.6@nd.edu

Abstract: Understanding the impact of molecular flexibility remains an important outstanding problem in rational drug design. Toward this end, we present new NMR relaxation methods that describe ligand flexibility at the atomic level. Specifically, we measure natural abundance ^{13}C cross-correlated relaxation parameters for ligands in rapid exchange between the free and receptor-bound states. The rapid exchange transfers the bound state relaxation parameters to the free state, such that a comparison of relaxation rates in the absence and presence of protein receptor yields site-specific information concerning the bound ligand flexibility. We perform these measurements for aromatic carbons, which are highly prevalent in drug-like molecules and demonstrate significant cross-correlated relaxation between the [13]C–[1]H dipole–dipole (DD) and ^{13}C chemical shift anisotropy (CSA) relaxation mechanisms. Our use of natural abundance measurements addresses the practical difficulties of obtaining isotope-labeled ligands in pharmaceutical research settings. We demonstrate our methods on a small ligand of the 42 kDa kinase domain of the p38 MAP kinase. We show that exchange-transferred cross-correlated relaxation measurements are not only sensitive probes of bound ligand flexibility but also offer complementary advantages over standard $R_1 = 1/T_1$ and $R_2 = 1/T_2$ measurements. The ligand flexibility profiles obtained from the relaxation data can help assess the influence of dynamics on ligand potency or pharmacokinetic properties or both, and thereby include inherent molecular flexibility in drug design.

Introduction

Flexibility is an inherent property of molecules that has been well established by both basic theory and experiment. Nevertheless, it has received comparatively scant attention in drug discovery programs when compared to that for molecular structure. As a consequence, we currently lack a predictive understanding of the relationship between inherent molecular flexibility and drug-like behavior. This limits our ultimate capacity to design novel therapeutics against novel targets. Thus, it is important to establish complementary experimental and theoretical approaches that can describe the molecular flexibility of ligands encountered in pharmaceutical research.

Toward this goal, we investigate here the use of natural abundance ^{13}C nuclear magnetic resonance (NMR) relaxation measurements to probe the dynamics of aromatic groups in ligands. Aromatic moieties are a highly prevalent class of chemical building blocks within all currently known drugs; thus, a focus on aromatic groups is well suited to pharmaceutical studies.[1] Additionally, we measure ^{13}C relaxation rate constants because a given rate constant reports directly on the reorientational motions of the corresponding CH bond vector. This contrasts with proton relaxation in which a given rate constant may depend on the dynamics of many interproton vectors.

Finally, we focus on *natural abundance* [13]C relaxation measurements. This focus reflects the practical difficulties of obtaining isotope-enriched small-molecule ligands in pharmaceutical research settings due to cost and synthetic complexity. Ligand-based NMR experiments that require ^{13}C-enriched ligands, however elegant, usually have rather limited utility.

Historically, ^{13}C relaxation measurements without isotope enrichment have been severely hindered by low natural abundance (~1.1%) and sensitivity ($\gamma_C/\gamma_H \approx 0.25$). While high-concentration samples (e.g. in excess of ~10 mM) can compensate, such concentrations are often unfeasible due to limiting solubility of ligand or protein or both in aqueous buffer. However, the advent of high-field magnets and cryogenic probes now provides the sensitivity for natural abundance measurements at concentrations more typical of ligand-based NMR pharmaceutical screens (~1 mM). Moreover, there is every indication that this sensitivity will increase. It is now reasonable to consider natural abundance ^{13}C relaxation experiments as a means to provide site-specific descriptions of ligand flexibility in pharmaceutical research. As proposed by Detlefsen et al., such "molecular flexibility profiles" can help relate molecular flexibility to the desirable properties of drugs.[2]

In what follows, we compare the natural abundance ^{13}C relaxation rates of ligand aromatic ^{13}C nuclei in the presence and absence of a target protein receptor. We focus on ligands

---

† Present address: Dept. of Chemistry and Biochemistry, University of Notre Dame, 251 Nieuwland Science Hall, Notre Dame, IN 46556-5670.

(1) Bemis, G. W.; Murkco, M. A. *J. Med. Chem.* **1996**, *39*, 2887–2893.

(2) Detlefsen, D. J. *Curr. Med. Chem.* **1999**, *6*, 353–383.

that exchange rapidly between the free and receptor-bound states; such ligands are typically encountered in NMR screening. In the presence of the receptor, we observe averaged ligand relaxation rates that reflect the transfer of the bound state rates to the free state via chemical exchange. The bound state rates can then be related to the bound ligand flexibility. Subsequent comparison with the free state rates yields an atomic-level description of the binding-induced changes in ligand flexibility and thus provides an avenue for assessing the influence of ligand conformational entropy in iterative drug design.

The first step in the characterization of bound ligand dynamics via exchange-averaged natural abundance ^{13}C relaxation was taken by Laplante et al. in their study of the NS3 protease domain of the hepatitis C virus.[3] Their studies focused solely on the use of the longitudinal ^{13}C relaxation rate constant $R_1 = 1/T_1$. However, exchange-averaged ^{13}C R_1 measurements have two potential drawbacks. First, R_1 ultimately decreases with increasing rotational correlation time (molecular weight). This means that the bound state R_1 can be less than that of the free state. Second, the bound state contribution to the average is scaled by the bound ligand fraction, P_B. Both considerations mean that under typical screening conditions in which $P_B \ll 1.0$, the bound state contribution to the exchange-averaged R_1 can be negligible. Accordingly, in this scenario, we obtain no information concerning the bound ligand flexibility. To increase the bound state sensitivity, we can measure instead the ^{13}C transverse rate constant $R_2 = 1/T_2$. In contradistinction to R_1, R_2 becomes amplified in the bound state due to its near proportionality to the overall rotational correlation time of the molecule. However, the exchange-averaged R_2 can also harbor "R_{ex}" contributions that originate from the nonequivalence of free versus bound chemical shifts. To extract the intrinsic bound state R_2, one must first correct for R_{ex}, and this can be nontrivial. Thus, both R_1 and R_2 measurements have drawbacks that can obfuscate the bound ligand dynamics. It is therefore essential to explore complementary relaxation parameters that can compensate.

Toward this end, we propose measurements of exchange-transferred *cross-correlated* relaxation rate constants at natural abundance. In particular, we are interested in the rate constants originating from the cross-correlation between the carbon chemical shift anisotropy (CSA) and ^{13}C$-^1$H dipole$-$dipole (DD) relaxation mechanisms in ^{13}C aromatic nuclei. Recent NMR studies of protein dynamics have pointed to the advantages of cross-correlated relaxation due to its independence from "R_{ex}" contributions in the fast exchange limit.[4,5] Additionally, like $R_2 = 1/T_2$, transverse cross-correlated relaxation parameters have a strong dependence on the overall rotational correlation time of the molecule and consequently become amplified in the receptor-bound state. Carlomagno et al.[6] and Blommers et al.[7] pioneered the use of exchange-transferred cross-correlated measurements for studies of bound ligand conformation. Carlomagno et al. used cross-correlations between pairs of ^{13}C$-$

^{1}H DD interactions to determine ribose ring conformations in ^{13}C-enriched nucleotide ligands. Blommers et al. used backbone ^{15}N$-^1$H/^{13}C$-^1$H DD and the ^{13}C$-^1$H DD/^{13}C=O CSA cross-correlations to determine bound peptide conformations. Both studies rely on the simultaneous presence of two isotopes of low natural abundance (i.e. pairs of ^{13}C nuclei or ^{15}N and ^{13}C nuclei), and therefore require isotope-enrichment of the ligand. However, as stated, the isotope-labeling requirement reduces significantly the general applicability of these approaches within pharmaceutical research settings, especially for non-peptide ligands.

The report proceeds as follows. In the Theoretical Considerations section we describe the dynamical information content of ^{13}C cross-correlation relaxation parameters and their behavior under two-state chemical exchange. We then describe new NMR methods to estimate the transverse CSA$-$DD cross-correlated relaxation rate constants for aromatic moieties in ligands at natural abundance. We demonstrate these methods on a small ligand interacting with the 42 kDa kinase domain of the p38 MAP kinase. Our results show that cross-correlated relaxation measurements can yield a profile of ligand flexibility in the bound and free states and localize binding-induced changes in flexibility. We further show that cross-correlated relaxation can be a more sensitive reporter of bound ligand flexibility than R_1, thus underscoring the need for complementary relaxation parameters. We conclude with a discussion of potential applications of these methods in drug design. This study represents part of a larger effort to establish new NMR methods for correlating ligand flexibility with desirable drug-like properties such as binding potency, selectivity, and oral bioavailability.

Theoretical Considerations

Aromatic Cross-Correlated Carbon Relaxation Rate Constants. For aromatic ^{13}C nuclei at natural abundance, the dominant relaxation mechanisms are the ^{13}C$-^1$H DD interaction, and the CSA of the aromatic carbon itself. Both mechanisms arise from second rank interaction tensors attached to the carbon in a molecular coordinate frame. Reorientational motion of these tensors due to molecular dynamics gives rise to local fluctuating fields that stimulate ^{13}C relaxation. Because the relative orientation of these tensors remains fixed, their corresponding local field fluctuations are correlated. This cross-correlation results in CSA$-$DD interference effects that enhance and retard the relaxation of the ^{13}C upfield and downfield doublet components, respectively.[8] We distinguish the upfield and downfield components with superscripts α and β, respectively, which specify the spin state ($|\alpha\rangle$ or $|\beta\rangle$) of the attached proton. We use $R^{\alpha/\beta}_2 = 1/T^{\alpha/\beta}_2$ and $R^{\alpha/\beta}_1 = 1/T^{\alpha/\beta}_1$ to denote doublet-specific transverse and longitudinal auto-relaxation rate constants. Accordingly, we can express transverse and longitudinal CSA$-$DD cross-correlated relaxation rate constants as the differences

$$\eta_z = \frac{1}{2} |R^{\alpha}_1 - R^{\beta}_1| \tag{1a}$$

$$\eta_{xy} = \frac{1}{2} | R^{\alpha}_2 - R^{\beta}_2| \tag{1b}$$

CSA$-$DD cross-correlated relaxation has been seized upon to

(3) LaPlante, S. R.; Aubry, N.; Deziel, R.; Ni, F.; Xu, P. *J. Am. Chem. Soc.* **2000**, *122*, 12530−12535.

(4) Brutscher, B.; Brüschweiler, R.; Ernst, R. R. *Biochemistry* **1997**, *36*, 13043−13053.

(5) Kroenke, C. D.; Loria, J. P.; Lee, L. K.; Rance, M.; Palmer, A. G., III. *J. Am. Chem. Soc.* **1998**, *120*, 7905−7915.

(6) Carlomagno, T.; Felli, I. C.; Czech, M.; Fischer, R.; Sprinzl, M.; Griesinger, C. *J. Am. Chem. Soc.* **1999**, *121*, 1945−1948.

(7) Blommers, M. J. J.; Stark, W.; Jones, C. E.; Head, D.; Owen, C. E.; Jahnke, W. *J. Am. Chem. Soc.* **1999**, *121*, 1949−1953.
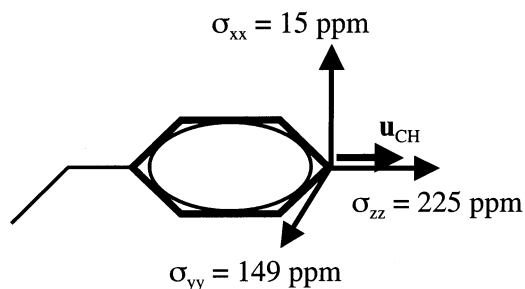
(8) Goldman, M. *J. Magn. Reson.* **1984**, *60*, 437−452.

Figure 1. Principal values and axes of the aromatic ^{13}C shielding tensor. The $\mathbf{u}_{CH}$ vector points along the CH bond, and the σ_{yy} principal axis lies in the aromatic plane.

study protein dynamics[5,9] and to enhance the sensitivity of NMR spectra of larger macromolecules via TROSY methods.[10]

The η_{xy} and η_z rate constants of a given CH bond provide dynamical information through their dependence on spectral density functions that describe the reorientational motions of the same CH bond. Letting $J^{CD}(\omega)$ designate the CSA−DD cross-correlation spectral density function, η_z and η_{xy} become[8]

$$\eta_z = CD_{CH}J^{CD}(\omega_C) \tag{2a}$$

$$\eta_{xy} = \frac{CD_{CH}}{6}\{4J^{CD}(0) + 3J^{CD}(\omega_C)\} \tag{2b}$$

where

$$J^{CD}(\omega) = a_{xx}J_X^{CD}(\omega) + a_{yy}J_Y^{CD}(\omega) \tag{3}$$

Thus, η_z and η_{xy} are linear combinations of $J^{CD}(\omega)$ evaluated at $\omega = 0$ and $\omega = \omega_C = \gamma_C B_o$. The shielding anisotropy prefactor is $C = \gamma_C B_o(2\sigma_{zz} - \sigma_{xx} - \sigma_{yy})$. D_{CH} is the heteronuclear dipolar coupling constant $\gamma_H\gamma_C(h/2\pi)/r_{CH}^3$. Subsequent discussions assume $r_{CH} = 1.09$ Å.[10] $J^{CD}(\omega)$ is a weighted sum of two spectral density functions, $J_X^{CD}(\omega)$ and $J_Y^{CD}(\omega)$. The weighting constants are $a_{xx} = C_{xx}/C$ and $a_{yy} = C_{yy}/C$, where $C_{xx} = \gamma_C B_o\cdot(\sigma_{zz} - \sigma_{xx})$ and $C_{yy} = \gamma_C B_o(\sigma_{zz} - \sigma_{yy})$. The two spectral density functions follow from the decomposition of the asymmetric ^{13}C shielding tensor into a sum of two axially symmetric tensors along orthogonal axes.[8] The symmetry axes of the two tensors correspond to the X and Y principal axes of the original tensor. Here, we adopt the tensor orientation and principal values of Veeman (cf. Figure 1).[11] Specifically, for each aromatic CH bond ($\mathbf{u}_{CH}$), the Z principal axis is parallel to the bond, while the X principal axis is orthogonal to the ring plane. The Y principal axis thus lies in the plane of the aromatic ring. The principal values are $\sigma_{zz} = 225$ ppm, $\sigma_{yy} = 149$ ppm, and $\sigma_{xx} = 15$ ppm.

$J_X^{CD}(\omega)$ and $J_Y^{CD}(\omega)$ are frequency distribution functions determined by the nature of the CH bond motions that reorient the CSA and DD interaction tensors. Models for the aromatic ring motion can provide analytical forms for $J_X^{CD}(\omega)$ and $J_Y^{CD}(\omega)$ in terms of various dynamical parameters. A compact formalism that accounts for both overall and internal molecular motion is that of Fischer et al. and Daragan et al.,[12,13] which is

an extension of the popular Lipari−Szabo "model-free" approach.[14,15] Specifically, for each CH bond, we assume time-correlation functions of the form

$$G_{X,Y}^{CD}(\tau) = \frac{1}{5}\exp(-\tau/\tau_{rot})\langle P_2(\mathbf{u}_{CH}(0)\cdot\mathbf{u}_{X,Y}(\tau))\rangle \tag{4}$$

$G_{X,Y}^{CD}(\tau)$ assumes isotropic overall tumbling characterized by τ_{rot}, and statistical independence between overall and internal motions. $P_2(x) = 1/2(3x^2 - 1)$ is the second-order Legendre polynomial, whose arguments are dot products between unit vectors $\mathbf{u}_{CH}$ and $\mathbf{u}_{X,Y}$. These unit vectors point along the aromatic CH bond and the X or Y principal axes of the ^{13}C shielding tensor, respectively. The angled brackets denote the molecular ensemble average. Thus, for each CH bond, $\langle P_2(\mathbf{u}_{CH}(0)\cdot\mathbf{u}_{X,Y}(\tau))\rangle$ measures the decay of equilibrium correlations between the orientations of two *different* unit vectors sampled at *different* times due to internal motion. Fourier transformation of eq 4 leads to the "model-free" spectral density functions

$$J_{X,Y}^{CD,MF}(\omega) = \frac{2}{5}\frac{\tau_{rot}S_{CHX,Y}^2}{1 + (\omega\tau_{rot})^2} +$$
$$\frac{2}{5}\frac{\{P_2(\mathbf{u}_{CH}\cdot\mathbf{u}_{X,Y}) - S_{CHX,Y}^2\}\tau_{eX,Y}}{1 + (\omega\tau_{eX,Y})^2} \tag{5}$$

Internal motions are parametrized by effective internal correlation times

$$\tau_{eX,Y} = \frac{\tau_{iX,Y}\tau_{rot}}{\tau_{iX,Y} + \tau_{rot}} \tag{6}$$

as well as order parameters

$$S_{CHX,Y}^2 = \langle P_2(\mathbf{u}_{CH}(0)\cdot\mathbf{u}_{X,Y}(\infty))\rangle \tag{7}$$

The order parameters $S_{CHX,Y}^2$ are limiting values of $\langle P_2(\mathbf{u}_{CH}(0)\cdot\mathbf{u}_{X,Y}(\tau))\rangle$ as $\tau \rightarrow \infty$; they describe the spatial restriction of correlated internal motions between the CH bond and the X or Y principal axes of the ^{13}C aromatic CSA tensor.

In the absence of internal motion, $P_2(\mathbf{u}_{CH}(0)\cdot\mathbf{u}_{X,Y}(\infty)) = P_2(\mathbf{u}_{CH}(0)\cdot\mathbf{u}_{X,Y}(0))$, and thus S_{CHX}^2 and S_{CHY}^2 reduce to the rigid tumbling limit of $P_2(\mathbf{u}_{CH}\cdot\mathbf{u}_{X,Y})$. Since we take the angles between $\mathbf{u}_{CH}$ and $\mathbf{u}_{X,Y}$ to be $\pi/2$, this is simply $-1/2$.[12,13] Thus, for an isotropic rigid tumbler, $J_X^{CD}(\omega) = J_Y^{CD}(\omega) = J_{X,Y}^{CD,ISO}(\omega)$, where

$$J_{X,Y}^{CD,ISO}(\omega) = \frac{2}{5}\frac{P_2(\mathbf{u}_{CH}\cdot\mathbf{u}_{X,Y})\tau_{rot}}{1 + (\omega\tau_{rot})^2} \tag{8}$$

On the other hand, the presence of internal motion can reduce the S_{CHX}^2 and S_{CHY}^2 magnitudes that, in turn, reduce the η_{xy} and η_z magnitudes. Larger amplitude internal motions yield larger reductions in the η_{xy} and η_z magnitudes.

The different dependencies of η_{xy} and η_z on the spectral density functions $J_X^{CD}(\omega)$ and $J_Y^{CD}(\omega)$ lend them distinctly different sensitivities to ligand binding (see, e.g. Peng, 2001).[16] Ligands toggle between the short τ_{rot} of the free state (e.g. τ_{rot}

(9) Tjandra, N.; Szabo, A.; Bax, A. *J. Am. Chem. Soc.* **1996**, *118*, 6986−6991.
(10) Pervushin, K.; Riek, R.; Wider, G.; Wüthrich, K. *J. Am. Chem. Soc.* **1998**, *120*, 6394−6400.
(11) Veeman, W. S. *Prog. Nucl. Magn. Reson. Spectrosc.* **1984**, *16*, 193−235.
(12) Fischer, M. W. F.; Zeng, L.; Pang, Y.; Hu, W.; Majumdar, A.; Zuiderweg, E. R. P. *J. Am. Chem. Soc.* **1997**, *119*, 12629−12642.

(13) Daragan, V. A.; Mayo, K. H. *J. Magn. Reson., Ser. B* **1995**, *107*, 274−278.
(14) Lipari, G.; Szabo, A. *J. Am. Chem. Soc.* **1982a**, *104*, 4546−4559.
(15) Lipari, G.; Szabo, A. *J. Am. Chem. Soc.* **1982b**, *104*, 4559−4570.
(16) Peng, J. W. *J. Magn. Reson.* **2001**, *153*, 32−47.

< 1 ns/rad) and the much larger τ_{rot} of the receptor (e.g. $\tau_{rot} >$ 10 ns/rad). Due to $J^{CD}(0)$, η_{xy} increases monotonically with τ_{rot} and, thus, molecular weight. As a result, η_{xy} becomes amplified in the bound state; this renders it a sensitive probe of the bound state even under large ligand excess. In contrast, η_z peaks at $\omega_C \approx 1/\tau_{rot}$ (~790 ps/rad at 18.8 T) and decreases for longer τ_{rot}. This means η_z will typically be smaller in the bound state and thus is an insensitive probe of the bound state under large ligand excess.

Behavior of Cross-Correlated Relaxation under Two-State Binding Exchange. Our focus is on the single-site binding equilibrium [E] + [L] $\leftrightarrow$ [EL], in which the ligand "L" exchanges between the free ([L]) and receptor-bound ([EL]) states with an exchange rate constant k_{ex}. The ligand–receptor association rate constant is $k_{on}[E] = P_B k_{ex}$, and the dissociation rate constant is $k_{off} = P_F k_{ex}$, where $P_B = [EL]/([L] + [EL])$ and $P_F = [L]/([L] + [EL])$ are the bound and free ligand fractions, respectively. We consider the effects of this exchange on the ligand η_{xy} since it is more sensitive to binding (vide supra). Unlike previous theoretical treatments of exchange-transferred cross-correlation, we do not start from the assumption of the fast-exchange.[6,7] Instead, we investigate by the behavior of η_{xy} over arbitrary exchange time scales using numerical simulations. This better enables us to understand the limits for the fast-exchange approximation that we ultimately invoke.

For a given ^{13}C doublet, the spin dynamics of a single-quantum coherence $C_+ = (C_x + iC_y)$ undergoing free precession, cross-correlated relaxation, and two-state exchange can be described by a system of rate equations $d\mathbf{V}/dt = -\mathbf{RV}$. $\mathbf{V}$ is column vector of spin orders that is the transpose of $\mathbf{V}^t = [\langle I^\beta C_{+,F}\rangle, \langle I^\beta C_{+,B}\rangle, \langle I^\alpha C_{+,F}\rangle, \langle I^\alpha C_{+,B}\rangle]$, and $\mathbf{R}$ is the four-by-four rate matrix

$$\mathbf{R}=\begin{bmatrix} R_{2,F}^\beta + P_B k_{ex} - i\Omega_F^\beta & -P_F k_{ex} & \mu_F & 0 \\ -P_B k_{ex} & R_{2,B}^\beta + P_F k_{ex} - i\Omega_B^\beta & 0 & \mu_B \\ \mu_F & 0 & R_{2,F}^\alpha + P_B k_{ex} - i\Omega_F^\alpha & -P_F k_{ex} \\ 0 & \mu_B & -P_B k_{ex} & R_{2,B}^\alpha + P_F k_{ex} - i\Omega_B^\alpha \end{bmatrix} \quad (9)$$

The subscripts "F" and "B" specify the free and bound ligand states. The free and bound state precession frequencies are $\Omega^{\alpha/\beta}_F = -|\omega_{C,F}| \pm \pi^1 J_{CH}$ and $\Omega^{\alpha/\beta}_B = -|\omega_{C,B}| \pm \pi^1 J_{CH}$, respectively. Henceforth, we let $\delta\omega = |\omega_{C,F} - \omega_{C,B}|$ denote the nonequivalence between the free and bound ^{13}C chemical shifts. The intrinsic relaxation rate constants of the free and bound state ^{13}C α/β doublets are $R^{\alpha/\beta}_{2,F}$ and $R^{\alpha/\beta}_{2,B}$, respectively (cf. eqs 1a,b). The μ_F and μ_B rate constants couple the relaxation of the α and β doublet components. Rigorous solution of $d\mathbf{V}/dt = -\mathbf{RV}$ involves diagonalizing $\mathbf{R}$. We pursue instead an approximate approach. Specifically, we note that the upper left and lower right quadrants of $\mathbf{R}$ simply constitute two sets of Hahn–Maxwell–McConnell (HMM) equations,[17,18] one set per doublet component, coupled by μ_F and μ_B. If we can safely neglect μ_F and μ_B, then $\mathbf{R}$ block-diagonalizes into two independent sets of HMM equations, each describing a two-state exchange process for the α/β component.

The μ_F and μ_B terms scramble the α and β identities. The scrambling manifests as cross-relaxation between the α/β components and causes the more rapid decay of antiphase versus in-phase transverse coherence. The μ_F and μ_B terms arise from

longitudinal $^1H-^1H$ dipole–dipole relaxation of the aromatic protons; as such, they increase with the overall rotational correlation time of the molecule and the local proton density. Therefore, $\mu_B \gg \mu_F$. The μ_B cross-term can be scaled down by perdeuteration of the protein target. One can also average out the $\mu_{F/B}$ effects with rf-pulse schemes (vide infra). Henceforth, we assume μ_F and μ_B are ~0 by either approach. Then, the upper left and lower right quadrants of $\mathbf{R}$ decouple into two independent two-state HMM exchange problems describing the α and β components, respectively. We assign each ^{13}C α/β doublet component an exchange-averaged transverse auto-relaxation rate, $R^{\alpha/\beta}_{2,av}$, derived from the well-known solutions of the two-state HMM equations.[19] Insertion of these $R^{\alpha/\beta}_{2,av}$ into the simple difference of eq 1b enables simulation of the exchange-averaged transverse cross-correlation rate $\eta_{xy,av}$ as a function of k_{off} for all exchange time scales. Explicit HMM rate expressions are given in the Supporting Information.

The result is Figure 2, which plots the exchange-averaged $\eta_{xy,av}$ versus log (k_{off}) under various conditions. All simulations assume a fixed ligand on-rate, $k_{on} = 1 \times 10^8$ M^{-1} s^{-1}, reasonable for diffusion-limited binding. Thus, the depicted k_{off} range corresponds to 1 μM $\leq K_D \leq$ 300 μM. In accordance with our experiments, the total protein and ligand concentrations are 50 μM and 1 mM, respectively. Both the free and receptor-bound ligands are treated as rigid isotropic tumblers with $J^{CD}(\omega)$ functions given by eq 8. The free and bound rotational correlation times are 150 ps and 20 ns, respectively. Finally, the nonequivalence between free versus bound ^{13}C chemical shifts is $|\delta\omega/2\pi| = 200$ Hz.

The lowest solid sigmoidal curve of Figure 2 depicts $\eta_{xy,av}$ based on the HMM $R^{\alpha/\beta}_{2,av}$ expressions. This curve assumes free-precession such as that occurring during a long Hahn spin–echo. The solid flat trace at the bottom represents the free state $\eta_{xy,F}$. Slow and fast exchange conditions prevail on the left and right sides of the vertical dashed line, respectively. The vertical dashed line indicates the k_{off} value satisfying the coalescence condition $k_{ex} = \delta\omega/(4P_FP_B)^{1/2}$.[20] The HMM curve obeys our intuitive expectations for the behavior of $\eta_{xy,av}$ with increasing ligand off-rate k_{off}. Under slow exchange, the ligand has long receptor residence times $\tau_{res} = k_{off}^{-1}$ during which the more rapid bound state relaxation can go to completion before the ligand dissociates. The $\eta_{xy,av}$ value thus scarcely deviates from the free state, leading to a negligible asymmetry between the α/β doublet relaxation rates. The correspondingly small deviation of $\eta_{xy,av}$ from $\eta_{xy,F}$ on the left-hand side of the vertical dashed line is evident in Figure 2. As k_{off} increases, the exchange becomes more rapid, and the bound state relaxation rate $\eta_{xy,B}$ is transferred more efficiently to the free state. As stated, the η_{xy} dependence on $J^{CD}(0)$ means $\eta_{xy,B} \gg \eta_{xy,F}$. Thus, the eventual increase of $\eta_{xy,av}$ with increasing k_{off} reflects the increasing contribution of bound state $\eta_{xy,B}$.

Generally, the chemical shift difference $\delta\omega$ does contribute to $\eta_{xy,av}$. To appreciate this, we consider the consequences of $\delta\omega \approx 0$. This can occur if the bound and free shifts are accidentally degenerate, if the exchange satisfies $k_{ex} \gg \delta\omega$ (fast exchange on the chemical shift time scale), or if the experiments explicitly remove the $\delta\omega$ relaxation effects. Examples of the

(17) Hahn, E. L.; Maxwell, D. E. *Phys. Rev.* **1952**, *88*, 1070.
(18) McConnell, H. M. *J. Chem. Phys.* **1958**, *28*, 430.

(19) Ni, F. *Prog. Nucl. Magn. Reson. Spectrosc.* **1994**, *26*, 517–606.
(20) Woessner, D. In *Encyclopedia of Magnetic Resonance*; Grant, D. M., Harris, R. K., Eds.; Wiley: Chichester, 1996; Chapter 6, pp 4018–4028.
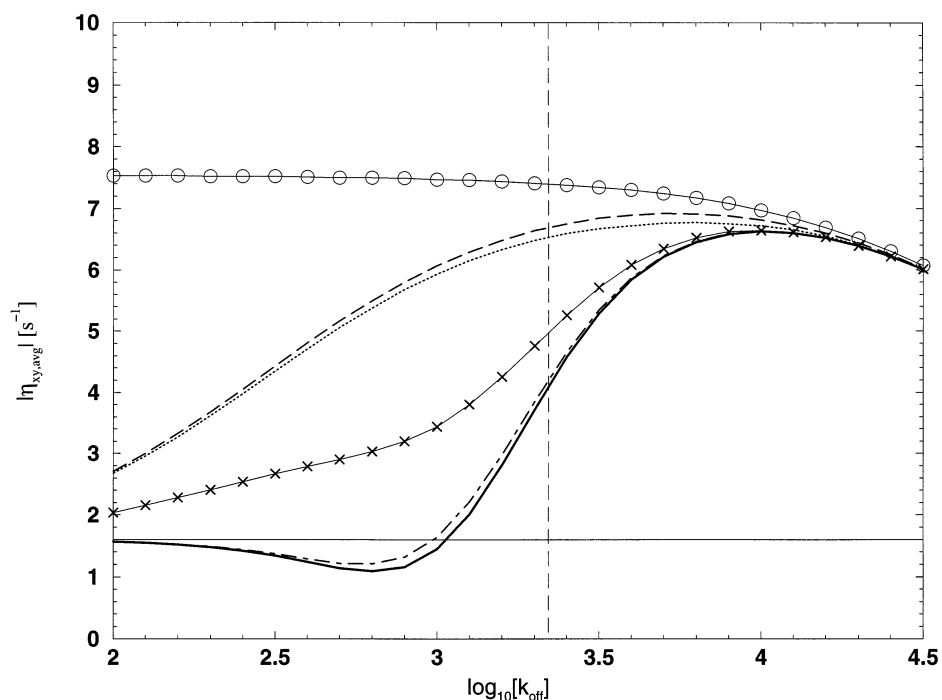
Figure 2. Simulations of the exchange-averaged transverse cross-correlated relaxation rate constant $|\eta_{xy,av}|$ versus log (k_{off}). The figure assumes a total protein concentration of 50 μM and a ligand concentration of 1 mM. Ligand–protein association is taken to be diffusion-limited with $k_{on} = 1 \times 10^8$ M^{-1} s^{-1}. Relaxation rates are calculated using simple Lorentzian spectral densities appropriate for rigid isotropic tumblers. The ligand and receptor rotational correlation times are 150 ps/rad and 20 ns/rad, respectively. The static field strength is $B_o = 18.8$ T (800 MHz proton frequency). The ^{13}C chemical shift difference between the free and bound ligand states is $\delta\omega/2\pi = 200$ Hz. The traces correspond to $|\eta_{xy,av}|$ calculated from the following expressions: solid: Hahn–Maxwell–McConnell; long-dashes: Swift–Connick with $\delta\omega = 0$; open-circles: fast-exchange average from eq 12 in the text. The Carver–Richards CPMG $\eta_{xy,av}$ traces are: dashed–dot: $t_{cp} = 20$ ms; x's: $t_{cp} = 2.5$ ms; dots: $t_{cp} = 0.5$ ms. The flat bottom trace is the free ligand value $\eta_{xy,F}$. The vertical dashed line is the k_{off} value at coalescence. Two protons within 2.5 Å of the considered proton are used for the free state, while six protons within the same distances were used for the bound state. The droop of the top trace at the largest k_{off} values reflects the decrease in the bound ligand fraction P_B as the k_{off} approaches $k_{on}[L_{tot}]$ (i.e. K_D approaches the total ligand concentration).

last situation include longitudinal relaxation and transverse spin-locking experiments employing strong effective rf fields. In Figure 2, the arc of long dashes above represents this $\delta\omega = 0$ limit. Clearly, for fixed k_{off}, suppression of $\delta\omega$ increases the $\eta_{xy,av}$ magnitudes relative to the more general case of $\delta\omega \neq 0$. An approximate expression for the $\delta\omega = 0$ curve is

$$\eta_{xy,av|\delta\omega=0} =$$
$$P_F\eta_{xy,F} + P_B\eta_{xy,B}\left\{\frac{(P_Fk_{ex})^2}{(R^\alpha_{2,B} + P_Fk_{ex})(R^\beta_{2,B} + P_Fk_{ex})}\right\} \quad (10)$$

Equation 10 follows easily from the Swift–Connick expressions and setting $\delta\omega = 0$ therein (see the Supporting Information). The Swift–Connick approximations are appropriate here since we focus on the major ligand species ($P_F \gg P_B$).[21] As with the more general case of $\delta\omega \neq 0$ (i.e. solid curve), larger k_{off} leads to larger $\eta_{xy,av}$ as a result of the increasing contribution of bound state $\eta_{xy,B}$.

At sufficiently large k_{off}, we pass to the fast exchange limit in which

$$R^{\alpha/\beta}_{2,av} = P_FR^{\alpha/\beta}_{2,F} + P_BR^{\alpha/\beta}_{2,B} + R_{ex} \quad (11)$$

Here, the $\delta\omega$ relaxation contribution enters via the additive R_{ex} term. However, when inserting eq 11 into eq 1b to calculate $\eta_{xy,av}$, the R_{ex} contributions die since they add equally to the α/β doublet components. The result is the simple population-

(21) Swift, T. J.; Connick, R. E. *J. Chem. Phys.* **1962**, *37*, 307–320.

weighted average

$$\eta_{xy,av} = P_F\eta_{xy,F} + P_B\eta_{xy,B} \quad (12)$$

first described by Carlomagno et al. and Blommers et al.[6,7] Therefore, under fast exchange, $\eta_{xy,av}$ is independent of R_{ex} (i.e., $\delta\omega$). This contrasts with conventional R_2 measurements, which, under identical exchange conditions, retain the R_{ex} contribution from eq 11. The top trace of open circles in Figure 2 illustrates the fast exchange $\eta_{xy,av}$ values from eq 12.

Figure 2 clearly shows that the fast-exchange trace is the upper limit as k_{off} increases for all $\eta_{xy,av}$ simulations. Thus, outside the fast-exchange limit (smaller k_{off}), $\eta_{xy,av}$ is *less* than that predicted by the simple average of eq 12. In general, $\eta_{xy,av}$ will have a complicated dependence on the intrinsic relaxation rates of the free and bound states, P_B, k_{off}, $\delta\omega$, and possibly an effective spin-lock field strength (vide infra). The convenient population-weighted average of eq 12 is valid only if the exchange is fast on both the chemical shift *and* the transverse relaxation time scales. On the chemical-shift time scale, fast exchange requires $k_{off} \gg |\delta\omega|$ (assuming $P_B \ll 1$). On the relaxation time scale, fast exchange requires $k_{off} = P_Fk_{ex} \gg R^\alpha_{2,B}$. This latter condition reflects the fact that $|R^{\alpha/\beta}_{2,B} - R^{\alpha/\beta}_{2,F}| \approx R^{\alpha/\beta}_{2,B}$, and that $R^\alpha_{2,B} > R^\beta_{2,B}$ for nonnegligible CSA–DD cross-correlation. In Figure 2, the long dashes representing eq 10 (i.e., $\delta\omega = 0$ case) generally lie below the fast-exchange open circles; this is a consequence of being outside the fast exchange regime on the relaxation time scale. Only at sufficiently large k_{off} do the two traces merge. Equivalently, if we

enforce $k_{off} = P_F k_{ex} \gg R^\alpha_{2,B}$ in eq 10, we reproduce the simpler fast exchange average of eq 12.

Cross-Correlated Relaxation in a Tilted Rotating Frame. Our experiments employ spin-locks that measure relaxation along an effective field tilted by angle Θ relative to the z-axis of the rotating frame. The angle Θ is related to the ^{13}C spin-lock field strength ω_1 and the resonance offset $2\pi\delta\nu$ through the well-known relation $\tan\Theta = |\omega_1/2\pi\delta\nu|$. The effective field magnitude is $\Omega = \sqrt{(\omega_1^2 + 4\pi^2\delta\nu^2)}$. If the spectral density functions $J_X^{CD}(\omega)$ and $J_Y^{CD}(\omega)$ do not vary rapidly for frequency excursions on the order of Ω, then $R_{1\rho} = \cos^2\Theta R_1 + \sin^2\Theta R_2 + \sin^2\Theta R_{ex}$. This leads directly to a rotating frame analogue of eqs 1a,b; namely,

$$\eta_{1\rho}(\Theta) = 0.5*(R^\alpha_{1\rho} - R^\beta_{1\rho}) \qquad (13)$$

such that

$$\eta_{1\rho}(\Theta) = \sin^2\Theta\ \eta_{xy}[1 + \cot^2\Theta\ (\eta_z/\eta_{xy})] \qquad (14)$$

To understand the effects of two-state exchange on $\eta_{1\rho}(\Theta)$, we need to assess its effects on $R_{1\rho}$ and then apply eq 13. Recently, Trott and Palmer have derived an $R_{1\rho}$ expression valid for arbitrary exchange time scales.[22] However, their expression does not explicitly account for the nonequivalence of intrinsic relaxation rates, which is clearly an important aspect of this study. The $R_{1\rho}$ expressions of Davis et al. do; however, their expression is restricted to fast exchange.[23] Nevertheless, in both cases, the terms relating explicitly to the nonequivalence of chemical shifts $\delta\omega$ and the spin-lock field strength are separate addends that contribute equally to the α/β doublet components. These contributions die in eq 13, resulting in

$$\eta_{1\rho,av} = P_F \eta_{1\rho,F}(\Theta_F) + P_B \eta_{1\rho,B}(\Theta_B) \qquad (15)$$

Equation 15 allows for different effective field tilt angles for the free and bound chemical shifts.[23] For spin-locks sufficiently strong $\omega_1 \gg \delta\omega$, and thus $\Theta_F \approx \Theta_B$. In the on-resonance condition $\Theta = \pi/2$, and $\eta_{1\rho,av}$ reduces to the simple average $\eta_{xy,av}$ of eq 12.

A general closed-form expression for $R_{1\rho}$ under two-state exchange that allows for the nonequivalence of both chemical shifts ($\delta\omega$) *and* intrinsic relaxation rate constants is not yet available. However, we can still get qualitative insight using simulations based on the Carver–Richards expressions for CPMG spin-locking, which do allow for both nonequivalencies (see the Supporting Information).[24] For example, if one uses long delays t_{cp} between consecutive 180° refocusing pulses, the resulting CPMG $\eta_{xy,av}$ values (cf. Figure 2, dashed–dotted sigmoidal curve, $t_{cp} = 20$ ms) nearly coincide with the sigmoidal HMM curve. This is reasonable, since long t_{cp} values correspond to a Hahn echo experiment. Shorter t_{cp} increases the effective field strength of the CPMG spin lock, $\sqrt{12}/t_{cp}$.[25] The resulting CPMG $\eta_{xy,av}$ magnitudes (cf. Figure 2, curve of "x's", $t_{cp} = 2.5$ ms) begin to increase. When t_{cp} becomes sufficiently short (i.e. $\sqrt{12}/t_{cp} > 10|\delta\omega|$), the CPMG spin lock field strength
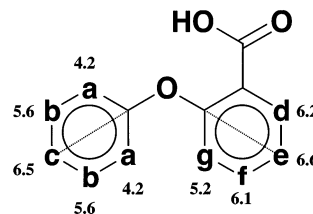

Figure 3. Schematic of the ligand **1**: 2-phenoxybenzoic acid. The compound is a specific binder to the ATP-binding site of the p38 MAP kinase with a $K_D \approx 70\ \mu M$. The bound state $P_B\eta_{xy,B}$ values estimated using eq 19 in the text are indicated next to appropriate carbons. The dashed lines highlight axes of internal rotation.

quenches the $\delta\omega$ relaxation contribution.[26] Accordingly, the consequent CPMG $\eta_{xy,av}$ values (cf Figure 2, dotted arc, $t_{cp} = 0.5$ ms) approach the arc of long dashes representing the $\delta\omega = 0$ condition of eq 10. The complexity of the Carver–Richards CPMG formulas implies an even more awkward expression for $\eta_{xy,av}$ under CPMG conditions. Fortunately, under sufficiently strong spin-locking fields (short t_{cp}) the comparatively simple eq 10 (the $\delta\omega = 0$ limit) can be used to analyze the data.

Materials and Methods

Samples. Measurements were performed on primarily two samples. One sample contained a small ligand, 2-phenoxybenzoic acid (**1**) at 1 mM, in the presence of 50 μM p38, a 42 kDa protein kinase. The kinase was overexpressed in *Escherichia coli* strain BL21(DE3), transformed with the p38 expression construct, and then purified chromatographically from the bacterial lysate. The ligand is part of our NMR screening library, which was purchased from commercial sources. A schematic of the ligand (**1**) is shown in Figure 3. For all samples, the buffer consisted of 10% D_2O, 90% H_2O, 50 mM P_i at pH 7.5.

General Aspects of NMR Measurements. All NMR spectra were recorded on an 800 MHz (18.8 T) Bruker Avance spectrometer at 278 K equipped with a standard triple-resonance inverse-detection probe having three axis gradients. Data processing used Xwinnmr2.5 (Bruker Biospin, Inc.). Ligand ^1H and ^{13}C assignments were determined using standard double-quantum filtered COSY,[27,28] dipsi-2 TOCSY,[29] and gradient versions of $^{13}C-{}^1H$ HSQC[30,31] and $^{13}C-{}^1H$ HMBC[32] experiments. Binding of **1** to p38 was demonstrated using the saturation transfer difference experiment.[33] Saturation involved a train of selective 90° Gaussian pulses applied for 2 s on the methyl signal region of p38 that was devoid of ligand resonances.

^{13}C Cross-Correlated Relaxation Measurements. Cross-correlated relaxation rate constants η_{xy} and η_z were measured using a two-dimensional (2D) $^{13}C-{}^1H$ correlation experiment schematized in Figure 4. Further details of the experiment are given below. Notably, the sequence uses adiabatic half-passage pulses to align magnetization along the effective field in the rotating frame.[34,35] The ^{13}C adiabatic pulses were of the tan/tanh form established by Mulder et al.[35] The frequency sweep initiated 26 000 Hz upfield from the center of the aromatic carbon spectrum and concluded slightly upfield of the furthest upfield resonance

(22) Trott, O.; Palmer, A. G., III. *J. Magn. Reson.* **2002**, *154*, 157−160.
(23) Davis, D. G.; Perlman, M. E.; London, R. E. *J. Magn. Reson., Ser B.* **1994**, *104*, 266−275.
(24) Carver, J. P.; Richards, R. E. *J. Magn. Reson.* **1972**, *6*, 89−105.
(25) Ishima, R.; Torchia, D. A. *J. Biomol. NMR* **1999**, *14*, 369−372.
(26) Deverell, C.; Morgan, R. E.; Strange, J. H. *Mol. Phys.* **1970**, *18*, 553−559.
(27) Piantini, U.; Sorensen, O.; Ernst, R. R. *J. Am. Chem. Soc.* **1982**, *104*, 6800−6801.
(28) Rance, M.; Sorensen, O. W.; Bodenhausen, G.; Wagner, G.; Ernst, R. R.; Wüthrich, K. *Biochem. Biophys. Res. Commun.* **1983**, *117*, 479−485.
(29) Shaka, A. J.; Lee, C. J.; Pines, A. *J. Magn. Reson.* **1988**, *77*, 274−293.
(30) Palmer, A. G., III; Cavanagh, J.; Wright, P. E.; Rance, M. *J. Magn. Reson.* **1991**, *93*, 151.
(31) Kay, L. E.; Keifer, P.; Saarinen, T. *J. Am. Chem. Soc.* **1992**, *114*, 10663−10665.
(32) Rinaldi, P. L.; Keifer, P. A. *J. Magn. Reson. A* **1994**, *108*, 259−262.
(33) Mayer, M.; Meyer, B. *Angew. Chem., Int. Ed.* **1999**, *38*, 1784−1788.
(34) Desvaux, H.; Berthault, P.; Birlirakis, N.; Goldman, M.; Piotto, M. *J. Magn. Reson. A* **1995**, 47−52.
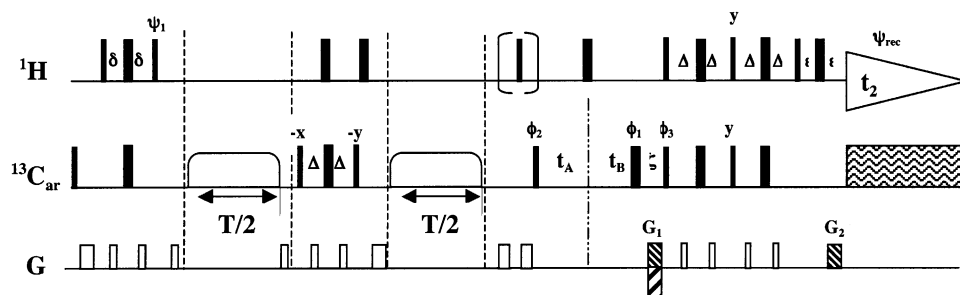(35) Mulder, F. A. A.; de Graaf, R. A.; Kaptein, R.; Boelens, R. *J. Magn. Reson.* **1998**, *131*, 351−357.

Figure 4. 2D $^{13}C-^{1}H$ pulse scheme for measuring $\eta_{1\rho}$. Thin and thick bars represent 90° and 180° pulses, respectively. Pulses without explicit phase labels are along $+x$. Phase cycling: $\phi_1 = +x, +y, -x, -y$; $\phi_2 = 4(+x)$, $4(-x)$, $\phi_3 = +x$, $\psi_1 = 2(+y)$, $2(-y)$, $\psi_{rec} = +x, -x, -x, +x, -x, +x, +x, -x$. Gradients critical for coherence selection are numbered. Frequency discrimination in $\omega_1(C)$ is obtained by inverting the sense of G_1 and ϕ_3 on alternate scans with subsequent echo/anti-echo data processing. G_1 and G_2 are 1 ms sine-shaped gradients applied at the magic angle with $G_1 = \pm 56$ G/cm and $G_2 = 14.1$ G/cm. Spin-lock pulses are indicated by open rectangles with rounded shoulders. The spin-locks are long CW pulses bracketed by 4 ms adiabatic tan/tanh pulses described in the text. For all experiments, the spin-lock field strength was set to 2570 Hz. The delays are $\Delta = 1/4J_{CH} \approx 1.5$ ms, $\delta = 1.3$ ms, $\epsilon = 1$ ms. The delay ξ accounts for the time needed for G_1. Two experiments are performed for a given value of T. One experiment detects C_z and sets $t_A = \Delta + t_1/2$, $t_B = t_1/2$, and the bracketed composite 90° pulse $(90_x 90_y)$ is turned on. The complementary experiment detects $2I_z C_z$ and sets $t_A = t_1/2$, $t_B = \Delta + t_1/2$ and the bracketed 90° pulse is turned off. Compensatory spin-locks at the beginning of the sequence (not shown) were used to prevent rf-heating artifacts. The 180° pulses between the two spin-locks and during the t_1 period are composite 90−180−90 pulses.

in the carbon spectrum (1415 Hz upfield from the spectral center). The spin-lock field strength was fixed at ∼2600 Hz. The strength of the ^{13}C spin-lock was determined by measuring the residual $^{1}J_{CH}$ splitting of a methine carbon in the presence of off-resonance continuous wave ^{13}C spin-locking. The residual splittings, J_r, were plotted as a function of ^{13}C carrier offset δ, and fitted to the functional form $J_r = {}^{1}J_{CH}\delta/\sqrt{(\omega_1{}^2 + \delta^2)}$.[36] To reduce heating effects, compensatory $R_{1\rho}$ spin-locks preceded the recycle delay such that the total power deposition remained constant for all relaxation time periods.[37]

For both the free ligand and ligand−receptor samples, five spin-locks were used, corresponding to relaxation delays $T = 40, 60, 80, 100$, and $120 (\times 2)$ ms. For each delay, two 2D spectra recorded separately the one-spin (256 scans per increment) and two-spin (1536 scans per increment) signal intensities $I_{one-spin}$ and $I_{two-spin}$ shown below in eq 16. The $I_{one-spin}$ and $I_{two-spin}$ intensities stem from the spin orders C_z and $2I_z C_z$, respectively; this is detailed further in the Results section (eq 18). The carbon sweep-width was set to 2900 Hz, and 16 complex points were acquired per 2D spectrum. The resulting acquisition time per 2D spectrum was 37.5 h and 6.5 h for the two-spin and one-spin spectra, respectively. For the free ligand, we performed η_z measurements using two methods. In the first method, we simply omitted the adiabatic pulses in Figure 4 and used identical relaxation delays. We then compared these results to those obtained using the established η_z pulse sequence of Kroenke et al.[5]

Cross-peak volumes from the one-spin and two-spin spectra were measured using xwinnmr 2.5 (Bruker Biospin, Inc.). The peak volumes were scaled to account for the different numbers of scans between the one-spin and two-spin spectra. For each resolved ^{13}C resonance, data files listing ratios of the resulting peak volumes $[I_{two-spin}/I_{one-spin}]$ versus relaxation delay T were fit to the single parameter function

$$[I_{two-spin}/I_{one-spin}](T) = \tanh(\eta T) \qquad (16)$$

where η was either $\eta_{1\rho}$ or η_z.[5,9] Parameter-fitting was performed via the Levenburg−Marquardt algorithm using in-house software. Equation 14 was used to extract η_{xy} values from $\eta_{1\rho}$ and η_z values. Duplicate spectra provided estimates of the statistical fluctuations in peak volumes, and the resulting uncertainties in the fitted cross-correlated rate constants were estimated using established Monte Carlo procedures (see e.g., Peng et al., 1992b).[38]

Longitudinal $R_1 = 1/T_1$ measurements. The pulse sequence for measuring ^{13}C $R_1 = 1/T_1$ was based on standard 2D proton-detected

sequences developed for AX spin systems.[39−42] Pulsed-field gradients were used for both coherence selection and water suppression. Suppression of CSA−DD cross-correlation during the relaxation delay was achieved with proton spin-inversion every 10 ms. For both protein-free and protein-containing samples, a series of 2D spectra were recorded with relaxation delays including 62.4, 124.8 (×2), 166.4, 208.0, 249.6, and 291.2 ms. Each 2D experiment consisted of 16 complex points with 256 scans per increment. Data reduction involved fitting 2D peak volume integrals (I) to the two-parameter single exponential form $I(T) = A \exp(-R_1 T)$ using the nonlinear least-squares and Monte Carlo procedures described above.

Results

Ligand−Receptor System. Our studies compare the natural abundance aromatic ^{13}C relaxation properties of a ligand exchanging between the bound and free states. The ligand is 2-phenoxybenzoic acid (**1**), which is a small molecule (214 Da) typical of our screening library. Figure 3 shows a schematic of (**1**) with the distinguishable carbon atoms labeled, and Figure 5 is a typical aromatic $^{13}C-^{1}H$ HSQC. The protein receptor is the 42 kDa catalytic domain of the p38 MAP kinase. The specific binding of **1** to the ATP-binding site of p38 has been established previously in our laboratory.[43] In particular, ^{1}H saturation transfer difference (STD) experiments[33] have demonstrated that **1** is a ligand of p38. Subsequent competition and fluorescence quenching experiments verified that the compound binds specifically to the intended kinase ATP-binding site with an equilibrium dissociation constant $K_D = 70$ μM. [43]

To probe the affects of receptor binding, we used two samples. One sample contained ligand at 1 mM in the presence of p38 at 50 μM. The 50 μM receptor concentration is typical of our transferred-NOE studies, and higher concentrations are often unfeasible due to aggregation. The NMR measurements on this sample were compared to those of a reference sample containing only the ligand in identical buffer. For this sample, we used 10 mM concentration to speed up the total measurement time. At this high concentration, one has to be concerned about

(36) Shaka, A. J.; Keeler, J. *Prog. Nucl. Magn. Reson. Spectrosc.* **1987**, *19*, 47−129.
(37) Wang, A. C.; Bax, A. *J. Biomol. NMR* **1993**, *3*, 715−720.
(38) Peng, J. W.; Wagner, G. *Biochemistry* **1992b**, *31*, 8571−8586.
(39) Nirmala, N.; Wagner, G. *J. Am. Chem. Soc.* **1988**, *110*, 7557−7558.
(40) Kay, L. E.; Torchia, D. A.; Bax, A. *Biochemistry* **1989**, *28*, 8972−8979.
(41) Boyd, J.; Hommel, U.; Campbell, I. D. *Chem. Phys. Lett.* **1990**, *175*, 477−482.
(42) Dayie, K. T.; Wagner, G. *J. Magn. Reson. A* **1994**, *111*, 121−126.
(43) Fejzo, J.; Lepre, C. A.; Peng, J. W.; Bemis, G. W.; Ajay; Murcko, M. A.; Moore, J. M. *Chem. Biol.* **1999**, *6*, 755−769.
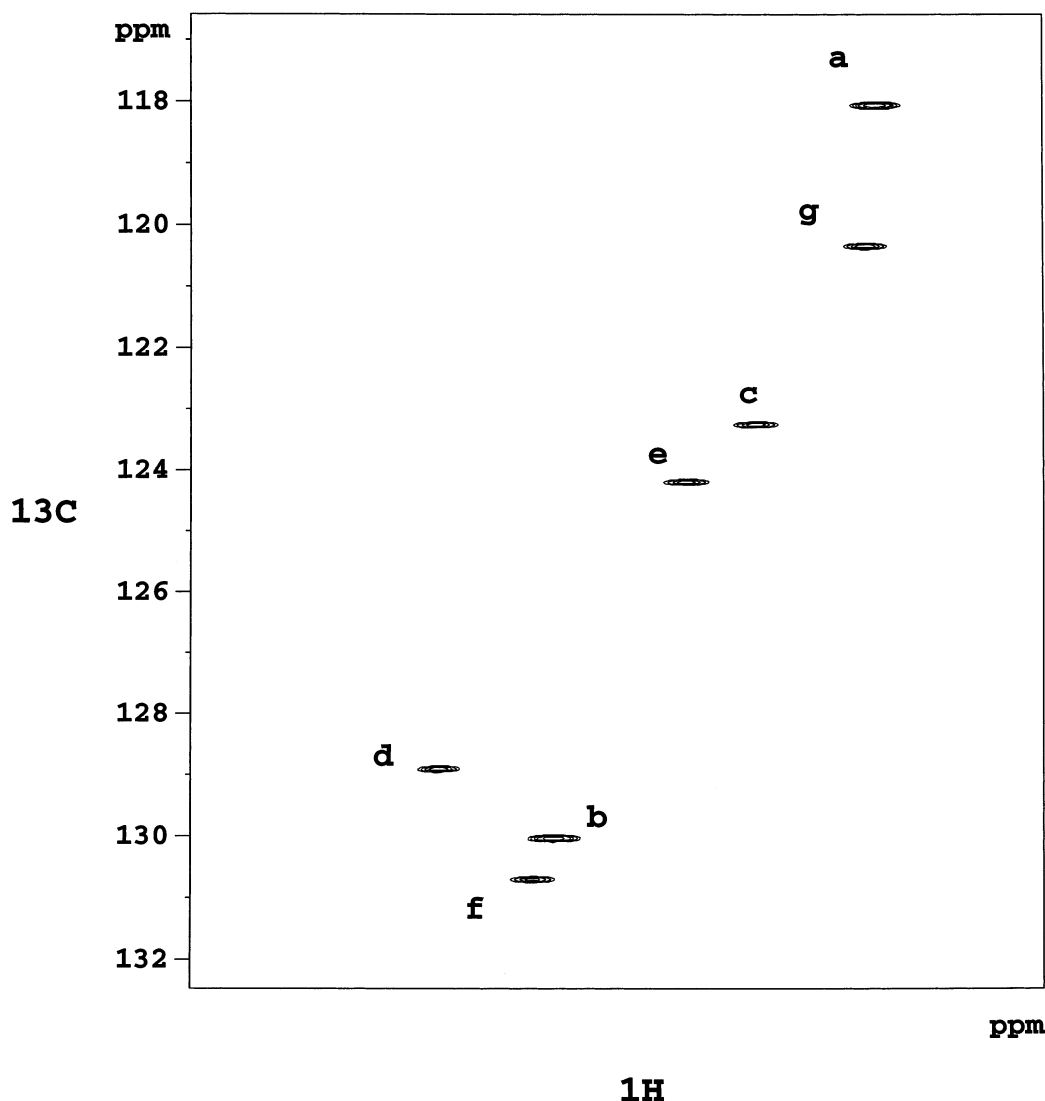
Figure 5. 2D $^{13}C-^1H$ HSQC of **1**. Cross-peaks are labeled according to the schematic of Figure 3.

the possibility of aggregation, which could lead to erroneous conclusions concerning the free ligand dynamics. No obvious aggregation was observed. However, to further allay anxieties of aggregation, we compared 2D NOESY spectra for the lone ligand at 10 mM versus 1 mM concentrations at 278 K. At both concentrations, a 400 ms NOE mixing period yielded cross-peaks that were negative or zero with respect to the diagonal. These results are consistent with the low molecular weight of the ligand and suggest that the higher 10 mM concentration does not enhance aggregation.

In both the absence and presence of p38, we observe only a single set of ligand resonances for both proton and carbon. This suggests but does not prove fast ligand exchange. On the other hand, the ligand $K_D \approx 70\ \mu$M and the assumption of diffusion-limited binding suggest an exchange rate constant $k_{ex} \geq 7300$ s^{-1}. This k_{ex} value exceeds the differences between the free and bound ^{13}C relaxation rates based on correlation times of 150 ps/rad and 20 ns/rad for the free and bound ligands, respectively. This suggests that such k_{ex} values are fast on the relaxation time scale. Since the aforementioned nonequivalence of ^{13}C chemical shifts, $\delta\omega$, is unknown, it is unclear whether k_{ex} satisfies the fast exchange condition of $k_{ex} > |\delta\omega|$. Given the estimated k_{ex},

our assumption of fast binding exchange is justified, provided the free versus bound ^{13}C shift differences are <0.6 ppm.

Cross-Correlated Relaxation as Sensitive Probes of Bound Ligand Relaxation. To assess the qualitative effects of binding on η_{xy}, we recorded a constant-time $^{13}C-^1H$ HSQC for **1** in the absence and presence of p 38. Figure 6 shows examples of the results. The spectra are $^1J_{CH}$-coupled along $\omega_1(^{13}C)$ to reveal the individual $^{13}C\ \alpha/\beta$ doublets. Due to the constant-time feature, the transverse relaxation rates of the doublet components are proportional to their peak heights. The vertical dashed lines select a representative ^{13}C doublet depicted in 1D fashion below. The doublet asymmetry is dramatically more pronounced in the presence of p38 (right panel B), and clearly demonstrates the enhanced relaxation of the upfield component. We observe an increase in doublet asymmetry for all CH bonds (i.e. $\eta_{xy,av} > \eta_{xy,F}$). In accordance with Figure 2, this is consistent with intermediate-to-fast binding exchange. For quantitative cross-correlated relaxation measurements, we used methods described in the next section.

Design of CSA−DD Cross-Correlated Relaxation Experiments. Tjandra et al. have developed 2D heteronuclear experiments to measure η_{xy} by monitoring the CSA−DD induced
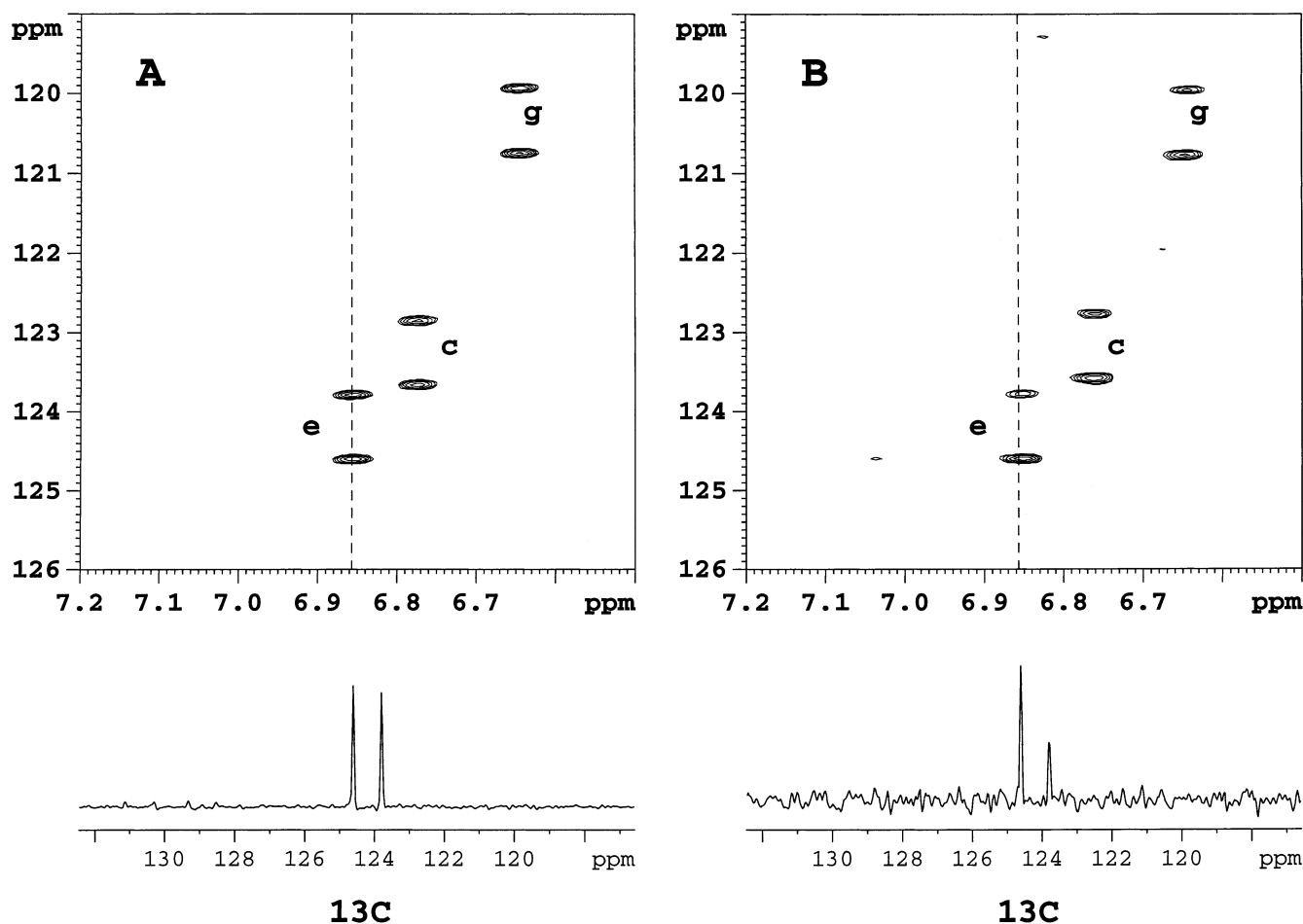
Figure 6. Comparison of ^{13}C doublets for **1** in the absence (A) versus presence (B) of p38. The vertical dashed line indicates an example doublet, resonance "e". The experiment is a ^{1}H-coupled constant-time HSQC.

cross-relaxation pathway $N_{xy} \leftrightarrow 2I_zN_{xy}$ for protein backbone $^{15}N-^{1}H$ bonds.[9] The $N_{xy} \leftrightarrow 2I_zN_{xy}$ cross-relaxation transpires during a Hahn echo. Differential precession of the α/β doublet components due $^{1}J_{NH}$ scalar coupling also averages out potential intra-doublet cross-relaxation; thus, the α/β components can be well approximated as relaxing independently (i.e. μ_F and $\mu_B =$ 0 cf. eq 9).

Transverse relaxation of *exchanging* nuclei can be enhanced by R_{ex} contributions, leading to a sensitivity loss during Hahn-echo segments that is especially harmful for natural abundance measurements. To minimize these losses, we have pursued cross-correlation measurements while spin-locking. Unfortunately, spin-locking suppresses the differential precession due to heteronuclear scalar coupling that had averaged out the intra-doublet cross-relaxation. Explicit averaging measures must therefore be adopted. To this end, we have incorporated the methods of Kroenke et al.[5] and Loria et al.,[44] in which a spin-echo at the midpoint of the relaxation period performs explicit averaging by inverting the sign of one doublet component relative to the other.

The CPMG pulse train remains a popular choice for spin-locking.[45,46] However, CPMG pulsing can suffer from significant off-resonance artifacts at high field strength B_o.[47,48] The aromatic

^{13}C sweep widths of pharmaceutical ligands can easily span 40 ppm, and the rf field strengths that would be required to meet the on-resonance condition for all aromatic carbons can endanger the sample and spectrometer. On the other hand, high-fields are advantageous for CSA−DD cross-correlation measurements since η_{xy} and η_z scale linearly with B_o. It is therefore desirable to have a spin-locking approach that permits cross-correlation measurements at high field. We have therefore adopted the off-resonance $R_{1\rho}$ method of Mulder et al.[35] This method uses an adiabatic half-passage pulse to align the magnetization of each aromatic carbon along its own effective field. A subsequent continuous-wave rf-field locks the magnetization along the effective tilted field in the rotating frame. Cross-correlated relaxation occurs along this tilted field with a characteristic rate constant rate $\eta_{1\rho}(\theta)$ that is related to η_{xy} and η_z through the simple trigonometric relation of eq 14.

The resulting pulse scheme is shown in Figure 4; it derives directly from extant pulse schemes for measuring backbone ^{15}N η_{xy} and R_{ex} values.[5,9,44] The magnetization flow is as follows. After the second ^{1}H 90° pulse with phase ψ_1, the density operator is $\sigma = 2I_zC_z$. In terms of single transition operators, we have $I^{\alpha}C_z - I^{\beta}C_z$ where $I^{\alpha} = 1/2(1 + 2I_z) = |\alpha\rangle\langle\alpha|$ and $I^{\beta} = 1/2(1-2I_z) = |\beta\rangle\langle\beta|$; thus, the upfield and downfield components are antiphase along the z-axis of the rotating frame.

(44) Loria, J. P.; Rance, M.; Palmer, A. G., III. *J. Biomol. NMR* **1999**, *15*, 151−155.
(45) Carr, H. Y.; Purcell, E. M. *Phys. Rev.* **1954**, *94*, 630.
(46) Meiboom, S.; Gill, D. *Rev. Sci. Instrum.* **1958**, *29*, 688.

(47) Czisch, M.; King, G. C.; Ross, A. *J. Magn. Reson.* **1997**, *126*, 154−157.
(48) Ross, A.; Czisch, M.; King, G. C. *J. Magn. Reson.* **1997**, *124*, 355−365.

Table 1. Relaxation Data (s^{-1}) for **1** −/+ p38 @ 18.8 T, 278K

CH bond	$^aR_{1,\mathrm{F}}$ (− p38)	$^bR_{1,\mathrm{av}}$ (+ p38)	$^c\eta_{z,\mathrm{F}}$ (− p38)	$^d\eta_{1\rho,\mathrm{F}}(\Theta)$ (− p38)	$^e\eta_{1\rho,\mathrm{av}}(\Theta)$ (+ p38)	$^f\eta_{xy,\mathrm{F}}$ (− p38)	$^gP_\mathrm{B}\eta_{xy,\mathrm{B}}$	$^hP_\mathrm{B}\eta_{xy,\mathrm{B}}/\eta_{xy,\mathrm{F}}$
a	1.32 ± 0.06	1.56 ± 0.19	0.57 ± 0.01	0.82 ± 0.02	5.00 ± 0.16	0.82 ± 0.02	4.17 ± 0.11	5.11 ± 0.16
b	1.55 ± 0.02	1.41 ± 0.11	0.59 ± 0.01	0.79 ± 0.01	3.83 ± 0.04	0.98 ± 0.02	5.57 ± 0.05	5.66 ± 0.09
c	1.62 ± 0.02	1.60 ± 0.12	0.85 ± 0.05	1.06 ± 0.01	6.52 ± 0.35	1.02 ± 0.02	6.49 ± 0.30	5.89 ± 0.28
d	1.83 ± 0.02	1.74 ± 0.24	0.63 ± 0.04	0.86 ± 0.02	4.48 ± 0.23	1.04 ± 0.03	6.15 ± 0.30	5.91 ± 0.33
e	1.84 ± 0.03	1.80 ± 0.13	0.68 ± 0.03	0.97 ± 0.05	6.21 ± 0.27	1.05 ± 0.04	6.58 ± 0.25	6.28 ± 0.34
f	2.01 ± 0.17	1.35 ± 0.06	0.95 ± 0.05	1.17 ± 0.02	4.33 ± 0.02	1.39 ± 0.05	6.08 ± 0.08	4.37 ± 0.16
g	1.64 ± 0.08	1.65 ± 0.05	0.61 ± 0.01	0.73 ± 0.02	5.67 ± 0.01	0.73 ± 0.02	5.17 ± 0.03	7.06 ± 0.15

^{a} Free ligand ^{13}C R_1. ^{b} Exchange-averaged ^{13}C R_1 in the presence of p38. ^{c} Free ligand longitudinal CSA−DD cross-correlated relaxation rate constant $\eta_{z,\mathrm{F}}$. ^{d} Free ligand rotating frame CSA−DD cross-correlated relaxation rate constant $\eta_{1\rho}(\Theta)$. ^{e} Exchange-averaged $\eta_{1\rho,\mathrm{av}}(\Theta)$ in the presence of p38. ^{f} Free ligand $\eta_{xy,\mathrm{F}}$ estimated from $\eta_{1\rho,\mathrm{F}}(\Theta)$ and $\eta_{z,\mathrm{F}}$. ^{g} $P_\mathrm{B}\eta_{xy,\mathrm{B}}$ estimated from $\eta_{1\rho,\mathrm{av}}(\Theta)$ and $\eta_{1\rho,\mathrm{F}}(\Theta)$.

Tan/tanh adiabatic pulses then rotate the doublet components $I^{\alpha/\beta}C_z$ to $I^{\alpha/\beta}(C_z \cos \Theta + C_y \sin \Theta)$. The doublet magnetization now lies along an effective spin-lock field tilted by the angle Θ away from the z-axis of the rotating frame. Cross-correlated relaxation ensues along the effective field for $T/2$, after which a time-reversed adiabatic pulse returns the ^{13}C magnetization to the z-axis. The aforementioned spin−echo sandwich then inverts the relative signs of the doublet components to reduce intra-doublet cross-relaxation.[44] The second ^{1}H 180° pulse after the sandwich restores the I^α and I^β identities established at the beginning of the sandwich. A second $R_{1\rho}$ spin-lock period follows for another duration $T/2$. After the second spin-lock, the density operator is

$$\sigma = I^\alpha C_z \exp[-R^\alpha_{1\rho}(\Theta)T] - I^\beta C_z \exp[-R^\beta_{1\rho}(\Theta)T] \quad (17)$$

Equation 17 assumes that intra-doublet cross-relaxation has been sufficiently suppressed such that the upfield and downfield components have relaxed independently at $R^\alpha_{1\rho}(\Theta)$ and $R^\beta_{1\rho}(\Theta)$, respectively, for a duration T. Rewriting eq 17 in Cartesian operators leads to

$$\sigma = \exp[-R_{1\rho}T]\{C_z \cosh(\eta_{1\rho}T) - 2I_zC_z \sinh(\eta_{1\rho}T)\} \quad (18)$$

The relaxation-weighted carbon magnetization is finally transferred to proton detection using the gradient-enhanced strategy for sensitivity-enhanced for coherence selection.[30,31] We select separately for the one-spin C_z versus two-spin $2I_zC_z$ terms using the strategy of Tjandra et al.[9] The results are two spectra per relaxation delay T with cross-peak intensities proportional to $\cosh(\eta_{1\rho}T)$ and $\sinh(\eta_{1\rho}T)$. The ratio of these cross-peak intensities as a function of T produces the hyperbolic tangent given by eq 16 (Materials and Methods). To estimate η_z, ($\Theta = 0$) we simply omit the spin-lock pulses.

Comparison of ^{13}C Cross-Correlated $\eta_{1\rho}(\theta)$ Rates. Using the pulse scheme of Figure 4, we first performed rotating frame $\eta_{1\rho}(\theta)$ measurements for the free ligand at 278 K. The spin-lock field strength was 2.6 kHz; the field strength was determined using the methods described above. The smallest effective field tip angle was ∼44° for resonance "f". The $\eta_{1\rho,\mathrm{F}}(\Theta_\mathrm{F})$ values ranged from 0.61 to 1.23 s^{-1} with an average estimated uncertainty of 0.03 s^{-1}. We then performed the same $\eta_{1\rho}(\Theta)$ measurements for the exchanging ligand in the presence of p38. We used the same spin-locking parameters as for the free ligand sample. The $\eta_{1\rho,\mathrm{av}}(\Theta)$ values now range from 3.83 to 6.52 s^{-1}, with an average estimated uncertainty of 0.15 s^{-1}. Thus, for all CH bonds, the $\eta_{1\rho}(\Theta)$ values increase significantly by factors ranging from 2.5- to 8-fold upon the addition of p38. These results are listed in Table 1 and depicted in Figure 7A.
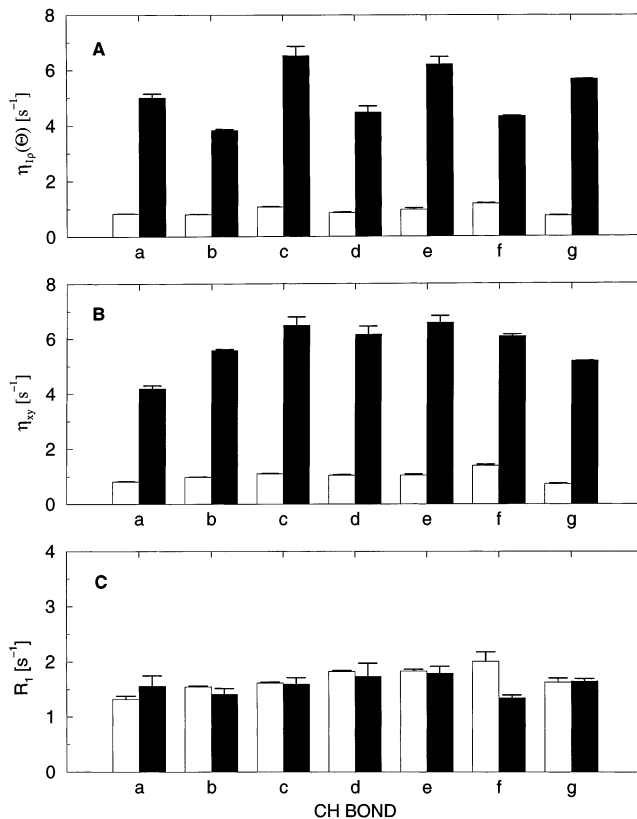

Figure 7. Comparison of natural abundance ^{13}C relaxation rates for **1** in the absence (clear bars) and presence (black bars) of p38. A: $\eta_{1\rho}(\Theta)$; B: η_{xy}. C: longitudinal relaxation rate constants $R_1 = 1/T_1$ For B, the bound state and free states are represented by $P_\mathrm{B}\eta_{xy,\mathrm{B}}$ and $\eta_{xy,\mathrm{F}}$ respectively.

The increases clearly exceed the estimated uncertainties. Note that the results for CH bonds "a" and "b" reflect population-weighted averages over pairs of ortho and meta positions. Figure 8 illustrates the more rapid build up of the $\tanh(\eta_{1\rho}T)$ ratio for representative CH bonds upon addition of p38, reflecting the increase of $\eta_{1\rho,\mathrm{av}}(\Theta)$ over $\eta_{1\rho,\mathrm{F}}(\Theta_\mathrm{F})$.

Estimates of the Bound Ligand Cross-Correlated η_{xy} Rates. We would ideally like to know $\eta_{xy,\mathrm{B}}$ since these rate constants report on the bound ligand flexibility. Comparisons of $\eta_{1\rho,\mathrm{av}}(\Theta)$ with $\eta_{1\rho,\mathrm{F}}(\Theta_\mathrm{F})$ can provide estimates of $\eta_{xy,\mathrm{B}}$ under certain assumptions. First, we assume that the magnitude of the ^{13}C chemical shift changes, $\delta\omega$, are substantially less than the rf-field strength ω_1, such that the tilt angles $\Theta_\mathrm{F} \approx \Theta_\mathrm{B} \approx \Theta$. Given that $\omega_1/2\pi \approx 2600$ hz, our angular approximation is reasonable provided the ^{13}C shift changes are ∼1−2 ppm. Next, we consider the aforementioned fact that η_z peaks at $\tau_{\mathrm{rot}} = 1/\omega_\mathrm{C}$ (∼790 ps/rad at 18.8 T), whereas the η_{xy} increases monotonically with τ_{rot}. A conservative estimate of the bound state correlation
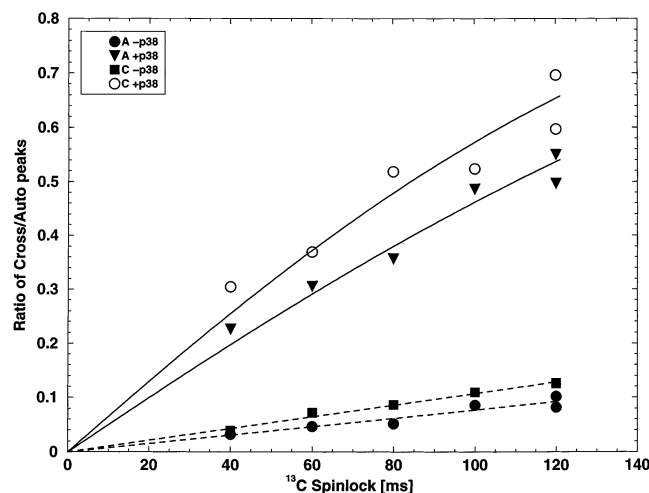
Figure 8. Examples of $\eta_{1\rho}(\Theta)$ build-up curves for CH bonds "a" and "c" obtained from the pulse sequence of Figure 4. Broken curves of circles ("a", ●) and squares ("c", ■) depict the build-up for the free ligand, and the solid curves of downward triangles ("a", ▼) and open circles ("c", ○) depict the more rapid build-up in the presence of p38.

time lies in the $10-20$ ns/rad range, while that of the free state lies in the $0.1-1$ ns/rad range. Accordingly, we assume that the magnitudes of $\eta_{1\rho,F}(\Theta_F)$ and $\eta_{z,B}$ are both much less than those of $\eta_{xy,B}$. Enforcing these assumptions in eq 15 yields

$$P_B\eta_{xy,B} \approx \frac{[\eta_{1\rho,av}(\Theta) - \eta_{1\rho,F}(\Theta)]}{\sin^2\Theta} \quad (19)$$

Equation 19 includes the bound ligand fraction P_B, which is the same for all CH bonds. Thus, even if P_B is unknown, we can still profile the relative flexibility of the bound ligand CH bonds. Table 1 lists the calculated values of $P_B\eta_{xy,B}$ for each CH bond of the ligand, and Figure 3 depicts these values next to the appropriate carbons.

Estimates of the Free Ligand Cross-Correlated η_{xy} Rates. To profile changes in ligand flexibility due to receptor-binding, we must compare the free ligand $\eta_{xy,F}$ values with the bound ligand $P_B\eta_{xy,B}$. The $\eta_{xy,F}$, values can be extracted from the free ligand $\eta_{1\rho,F}(\Theta)$ data, provided we correct for $\eta_{z,F}$. Unlike the bound state, $\eta_{z,F}$ is expected to be comparable to $\eta_{xy,F}$ due to the short overall correlation time of the free ligand which tends to equalize $J^{CD}(\omega_C)$ and $J^{CD}(0)$. We therefore measured $\eta_{z,F}$ directly using two methods. In the first method, we simply omitted the adiabatic pulses and spin-locks in the pulse sequence of Figure 4. In lieu of a spin-lock, the tilt angle is $\Theta = 0$, and the sequence monitors the longitudinal CSA−DD cross-relaxation pathway $C_z \leftrightarrow 2I_zC_{zz}$. In a second method, we used the established pulse sequence of Kroenke et al.[5] This sequence uses two averaging periods instead of one to better ensure $\mu_F = 0$ (cf. eq 9). We compared the $\eta_{z,F}$ values from both methods and found them to agree within experimental error. The agreement is consistent with the notion that μ_F is small in the free state. Of course, such an agreement cannot be expected for a substantially larger molecule. Table 1 lists the $\eta_{z,F}$ values from the method of Kroenke et al.[5] The $\eta_{z,F}$ values ranged from 0.43 to 0.91 s^{-1} with an average uncertainty of 0.03 s^{-1}. Application of eq 14 yielded the resulting $\eta_{xy,F}$ values, which ranged from ∼0.62 to 1.6 s^{-1}, with an average uncertainty of ∼0.03 s^{-1}. Figure 7B juxtaposes the free state $\eta_{xy,F}$ and the bound state $P_B\eta_{xy,B}$ for comparison.

Comparison of Ligand ^{13}C Longitudinal Relaxation Rates. As stated, LaPlante et al., have recently proposed exchange-transferred longitudinal ^{13}C relaxation rates ($R_1 = 1/T_1$) at natural abundance to pinpoint binding-induced changes in ligand flexibility.[3] Their measurements were performed on a peptide ligand at $3-4$ times the concentration of the ligand studied here and, in the presence of 50 μM of its binding receptor, the NS3 domain of the hepatitis C protease. To compare the sensitivities of R_1 and the cross-correlated relaxation measurements to binding, we also performed ^{13}C R_1 measurements.[42] Table 1 lists the R_1 values and the estimated uncertainties, and Figure 7C displays the corresponding bar chart. For the lone ligand, the R_1 values range from 1.32 to 2.01 s^{-1} with an average error of 0.06 s^{-1}. In the presence of p38, the ligand R_1 values lie in the range of $1.3-1.8$ s^{-1}, with an average error of 0.13 s^{-1}. Thus, the presence of receptor does not significantly change R_1. The larger estimated errors of the p38/ligand sample reflect the lower signal-to-noise spectra of the more dilute sample.

Discussion

Bound Ligand Flexibility. A comparison of the $\eta_{1\rho,av}(\Theta)$ and $\eta_{1\rho,F}(\Theta)$ data provides estimates of the bound state $P_B\eta_{xy,B}$. $P_B\eta_{xy,B}$ is of interest since it reports on the bound ligand flexibility. To evaluate the plausibility of our results, we set $P_B = 0.05$, based on the aforementioned ligand K_D of 70 μM and the prevailing ligand and protein concentrations. The resulting $\eta_{xy,B}$ range from 89 to 135 s^{-1}, with a mean value of 119 s^{-1}. If we momentarily treat the maximum $\eta_{xy,B}$ value as coming from a ligand bound rigidly within an isotropically tumbling protein, then the implied correlation time for p38 would be ∼20 ns/rad. Previous studies of kinase domain dynamics suggest that this value is reasonable for a protein the size of p38.[49,50]

If the ligand were rigidly bound to an isotropically tumbling protein, we would expect uniform $P_B\eta_{xy,B}$ values. Instead, Figure 7B shows significant $P_B\eta_{xy,B}$ variation among the CH bonds. This is further evident in Figure 3, which annotates the aromatic carbons with their $P_B\eta_{xy,B}$ values. Under the assumption of overall isotropic tumbling, these variations suggest residual bound state motion of the ligand. In the context of the "model-free" spectral density functions $J_{X,Y}^{CD,MF}(\omega)$ (cf. eq 5), residual ligand motion in the bound state can reduce the magnitudes of the bound state order parameters S^2_{CHX}, S^2_{CHY}, which, in turn, reduces the $\eta_{xy,B}$ magnitude from that predicted by rigid docking. Larger amplitude CH bond motions lead to smaller values of $P_B\eta_{xy,B}$. A plot of $P_B\eta_{xy,B}$ as function of CH bond (cf. Figure 7B) therefore yields a profile of the bound ligand flexibility. In this profile, CH bonds "a" and "g" experience greater internal motion in the bound state, while CH bonds "c" and "e" experience the least. Such motion could consist of internal torsion angle fluctuations as well as restricted rigid body rotations of the entire ligand within the ATP-binding site ("rattling-in-a-cage" motion). Structures of **1** complexed with p38 are not available. However, examination of crystal structures of p38 in complex with larger tight inhibitors suggests the available volume within the ATP-binding site significantly exceeds that of the ligand (**1**) (B. Hare, personal communication). Thus, it is conceivable that the ligand could at least "rattle" within the ATP cage.

(49) Seifert, M. H.; Breitenlechner, C. B.; Bossemeyer, D.; Huber, R.; Holak, T. A.; Engh, R. A. _Biochemistry_ **2002**, _41_, 5968−5977.
(50) Gangal, M.; Cox, S.; Lew, J.; Clifford, T.; Garrod, S. M.; Aschbaher, M.; Taylor, S. S.; Johnson, D. A. _Biochemistry_ **1998**, _37_, 13728−13735.

We note that $\eta_{xy,B}$ is sensitive not only to the amplitude of the internal motion, but also on its directional properties.[12,13] As stated, in the absence of internal motion, S^2_{CHX} and S^2_{CHY} reduce to the rigid tumbling limit $P_2(\mathbf{u}_{CH}\cdot\mathbf{u}_{X,Y}) = -1/2$. However, even in the presence of internal motion, the same rigid-tumbling limit can be achieved if that internal motion occurs along certain directions. As shown in eq 7, S^2_{CHX} and S^2_{CHY} consider the ensemble average of the angle between two *different* unit vectors considered at *different* times. If the internal ligand motions leave the angle between the unit vectors $\mathbf{u}_{CH}(0)$ and $\mathbf{u}_{X,Y}(\tau)$ invariant, then the only source of de-correlation is overall molecular tumbling; hence, the order parameters adopt the rigid tumbling limits. An example would be torsion angle motion about an axis collinear with a given CH bond vector. Such motion would reorient $\mathbf{u}_X$ and $\mathbf{u}_Y$, but not $\mathbf{u}_{CH}$; thus, this motion would not affect the η_{xy} of the corresponding CH bond. It follows that larger $P_B\eta_{xy,B}$ values can also reflect collinearity between the $\mathbf{u}_{CH}$ unit vector and an axis of internal rotation. In this context, it is interesting to note that the "c" and "e" CH bonds lie along the intuitive axes of internal torsional rotation, and therefore it is tempting to attribute their larger $\eta_{xy,B}$ values to their privileged orientations along these putative internal rotation axes (dashed lines in Figure 3).

We must also recall that S^2_{CHX} and S^2_{CHY} need not be equal. Equality would imply isotropic local motion.[12] While this may be possible, the local motional anisotropy clearly depends on the binding mode. The possibility of describing motional anisotropy of the ligand is intriguing because it represents novel information for medicinal chemistry. Strategies for describing the anisotropic motions of rigid fragments in proteins and peptides have been described by Fischer et al. and Bremi et al. and involve extensive measurements of auto- and cross-correlated relaxation rates.[12,51] Analogous analyses would be desirable for bound ligands. However, here we have only limited relaxation data on the bound state; namely, one relaxation parameter ($P_B\eta_{xy,B}$) per CH bond. By itself, the data here are insufficient for an analysis in terms of the "model-free" order parameters S^2_{CHX} and S^2_{CHY} shown in $J^{CD,MF}_{X,Y}(\omega)$ (cf. eqs 5–7).

To be able to test motional models, there are several approaches we might consider. First, we can measure additional relaxation parameters. For example, backbone relaxation experiments can be performed on receptor protein enriched with ^{15}N to directly determine the overall rotational correlation time of the bound state, $\tau_{rot,B}$. Second, we might consider η_{xy} measurements at different field strengths, B_o. However, a key asset of η_{xy} is its bound state sensitivity under a large free ligand excess on account of its $J^{CD}(0)$ dependence (cf. eq 2b). Therefore, the bound state information is transferred primarily via $J^{CD}(0)$, which is B_o-independent. And although η_{xy} would scale linearly with B_o, we would not obtain new frequency information about $J^{CD}(\omega)$ necessary to test motional models. A third avenue is a molecular dynamics analysis of the ligand–receptor complex. From simulated rotational fluctuations of the aromatic ring fragments, one can calculate CSA–DD cross-correlation functions and spectral densities and, thus, simulated η_{xy} rate constants that can be compared with experiment. The appeal of this approach is the potential for gaining a detailed description of ligand flexibility beyond order parameters.[52,53]
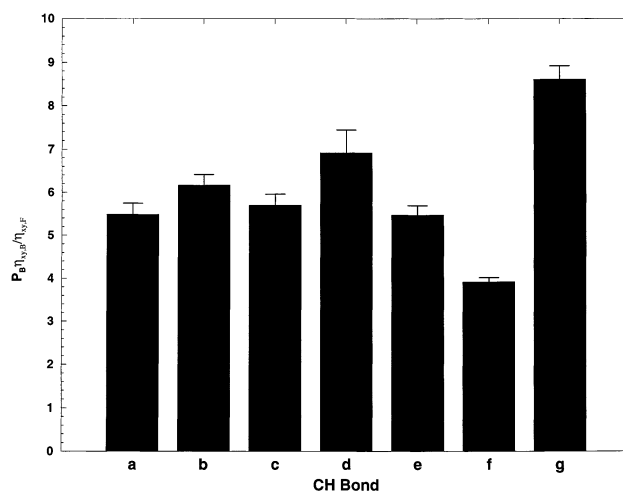

Figure 9. Ratios $P_B\eta_{xy,B}/\eta_{xy,F}$ for **1**.

While deeper interpretation awaits further experiment or analysis or both, it is important to recognize that the ability to compare metrics of ligand flexibility, in and of itself, is still useful for pharmaceutical research. Metrics of flexibility, while not necessarily being complete descriptions of the dynamics, can nevertheless be instructive when compared across a series of analogues because they can enable a correlation between differences in flexibility with differences in biological activity. The CSA–DD cross-correlated relaxation measurements discussed here are examples of such metrics.

Binding Induced Changes in Ligand Flexibility. It is also interesting to determine whether receptor binding changes the internal ligand flexibility. Indeed, the observed variation of $\eta_{xy,F}$ and $\eta_{z,F}$ with CH bond for the free ligand suggests internal flexibility. In particular, the monotonic increase of η_{xy} one observes from CH bond "a" to "b", and to "c" is evident in both the $\eta_{xy,F}$ and $P_B\eta_{xy,B}$. To compare more clearly the η_{xy} profiles of the free versus bound ligand, we consider the ratios $P_B\eta_{xy,B}/\eta_{xy,F}$. Figure 9 plots these ratios versus CH bond. If the flexibility profile is unchanged between the free and bound states, then the bound ligand $\eta_{xy,B}$ profile would essentially just be a scaled-up version of the free ligand $\eta_{xy,F}$ profile due to its longer overall correlation time. Consequently, $P_B\eta_{xy,B}/\eta_{xy,F}$ would be approximately the same for all CH bonds. However, Figure 9 reveals that the $P_B\eta_{xy,B}/\eta_{xy,F}$ ratios are not uniform and suggests the binding is more complex than the union of two rigid isotropic tumblers. In the context of $J^{CD,MF}_{X,Y}(\omega)$ (cf. eqs 5–7), the $P_B\eta_{xy,B}/\eta_{xy,F}$ ratio is ostensibly a function of all free and bound motional parameters. However, if we assume isotropic tumbling, then $\tau_{rot,B}$ and $\tau_{rot,F}$ are the same for all CH bonds. Therefore, nonuniform $P_B\eta_{xy,B}/\eta_{xy,F}$ ratios reflect differential changes in the *internal* flexibility parameters ($S^2_{CHX,Y}$ and $\tau_{e,X,Y}$) upon receptor binding. For example, CH bonds that retain greater mobility in the bound state may have reduced magnitudes for S^2_{CHX} and S^2_{CHY} (the reduction being subject to the local motional anisotropy). Such CH bonds will display smaller $P_B\eta_{xy,B}/\eta_{xy,F}$ than those that rigidify upon binding. Alternatively, CH bonds that experience greater free state mobility will show the same trend due to their smaller $\eta_{xy,F}$ values. Comparisons of $P_B\eta_{xy,B}/\eta_{xy,F}$ can therefore map the

(51) Bremi, T.; Brüschweiler, R. *J. Am. Chem. Soc.* **1997**, *119*, 6672–6673.

(52) Bremi, T.; Brüschweiler, R.; Ernst, R. R. *J. Am. Chem. Soc.* **1997**, *119*, 4272–4284.
(53) Lienin, S. F.; Brüschweiler, R. *Phys. Rev. Lett.* **2000**, *84*, 5439–5442.

relative binding-induced changes in flexibility onto the ligand structure. In this perspective, Figure 9 suggests similar extents of rigidifcation for CH bonds "a−e", while lesser and greater changes occur for CH bonds "*f*" and "*g*", respectively.

Comparison of Transferred R_1 and $\eta_{1\rho}(\Theta)$ Measurements. The increases in $\eta_{1\rho}(\Theta)$ induced by the addition of p38 are obvious in Figure 7A. These results clearly demonstrate that $\eta_{1\rho}(\Theta)$ is sensitive to the bound state relaxation properties of the ligand. The strong response of $\eta_{1\rho}(\Theta)$ contrasts starkly with the essentially invariant R_1 measurements. As seen in Figure 7C, the addition of p38 induces no significant differences in the ligand R_1. Only CH bond "*f*" shows a significant decrease of ~33%. Clearly, for our studies here, a reliance on R_1 alone would miss some of the internal ligand dynamics suggested by $P_B\eta_{xy,B}$ in Figure 7B. These results suggest that exchange-transferred R_1 may not always be sensitive to the bound state ligand relaxation and, hence, the bound state dynamics. These results makes sense, given that R_1 has a similar dependence as η_z on the effective rotational correlation time; that is, the bound state $R_{1,B}$ can be much less than $R_{1,F}$. Due to the saturating amounts of ligand ($P_F \gg P_B$) the bound state contribution ($P_B R_{1,B}$) to the fast-exchange average $R_{1,av} = P_F R_{1,F} + P_B R_{1,B}$ can become negligibly small. Of course, R_1 will not always be insensitive to the bound ligand dynamics. The free ligand could possess internal motions in the extreme narrowing regime ($\tau \ll 1/\omega_C$) that become restricted in the bound state, leading to a longer effective correlation time $\tau \approx 1/\omega_C$. In such cases, the $R_{1,B}$ might be $> R_{1,F}$. However, such scenarios cannot be generalized. Exchange-transferred R_2 measurements are sensitive reporters of the bound state, even when $P_B \ll 1.0$, since R_2 is proportional to the overall rotational correlation time. However, interpretation of the fast exchange R_2 values can be complicated by R_{ex} contributions stemming from the nonequivalence of free versus bound ^{13}C chemical shifts, $\delta\omega$.

In this context, the appeal of η_{xy} becomes clear. Like R_2, η_{xy} has a strong dependence on the effective overall rotational correlation time on account of $J^{CD}(0)$ (cf. eq 2b). This means that even in the presence of a free ligand excess, $\eta_{xy,av}$ (cf. eq 12b) effectively conveys the bound state relaxation properties and, thus, bound state dynamics. However, unlike R_2, η_{xy} does not harbor R_{ex} in the fast-exchange limit and is therefore easier to interpret. We note, however, that measurements of R_2 and other transverse autorelaxation rates, such as those of multiple quantum (MQ) coherence, could still prove informative when combined with η_{xy} measurements. More specifically, a combined analysis of η_{xy} and R_2 (or R_{MQ}) data could help distinguish R_{ex} contributions to the latter. The joint set of relaxation rates would then enable a testing of motional models for the bound state dynamics that would be unfeasible using either measurement alone.

Caveats. We have assumed fast exchange both with respect to the chemical shifts and intrinsic relaxation time scales. This assumption is based on a binding exchange rate constant, k_{ex}, for **1** that exceeds reasonable estimates of ^{13}C relaxation rates and binding-induced chemical shift differences. A single set of resonances in the presence and absence of p38, and the increase of η_{xy} in the presence of p38 further supports this assumption. However, without independent estimates of the binding-induced shifts, $\delta\omega$, we must keep in mind that the exchange-averaged η_{xy} values might be less than the simple population-weighted

averages of eqs 12 and 15 (cf. Figure 2). In an initial attempt to query this, we repeated the constant-time $^{13}C-{^1H}$ correlation experiment shown in Figure 6 for both the free ligand and the ligand/p38 sample at a higher temperature of 288 K, with the aim of increasing the exchange rate. No significant increases in doublet asymmetry were observed, consistent with the notion that the exchange is already fast at 278 K.

In principle, we should also account for the possibility of intra-ligand exchange. Obvious examples are the "a" and "b" CH bonds, which exchange among two ortho and meta sites connected by 180° ring flips. This could cause additional $\delta\omega$ relaxation contributions that further enhance the α/β transverse relaxation. Thus, we assume here that $\delta\omega$ relaxation contributions from on/off exchange dominate those from the intra-ligand exchange. However, theoretical studies of exchange-averaged $R_{1\rho}$ suggest that, unless the intrinsic rate constants vary dramatically between the putative intra-ligand states, the $\delta\omega$ contribution will still be an addend that contributes equally to the α/β doublet components.[22] In this case, the simple averages of eq 12 and 15 would still apply.

We have described aspects of the η_{xy} data in terms of the "model-free" approach. A basic assumption of this approach is that the overall and internal motions are statistically independent because they occur on vastly different time scales. This assumption is reasonable for slowly tumbling molecules such as receptor-bound ligands. However, it may not reasonable for small ligands tumbling rapidly in free solution. Thus, any future "model-free" analyses of free ligand must be interpreted with caution.

We have also assumed that the ^{13}C aromatic CSA tensors adopt the same orientation and principal values in the free and bound states. If we lift this assumption, then some of the binding-induced changes in η_{xy} may reflect a toggling between different CSA tensors (i.e. free versus bound). Specifically, eqs 2−3 show that changes in the CSA principal values will scale η_{xy} via the prefactors C, a_{xx} and a_{yy}. Changes in tensor orientation can alter the Legendre terms $P_2(\mathbf{u}_{CH}\cdot\mathbf{u}_{X,Y})$ and $\langle P_2(\mathbf{u}_{CH}(0)\cdot\mathbf{u}_{X,Y}(\tau))\rangle$ in eqs 4, 5, and 8, thereby altering the rigid-body magnitude of η_{xy}, as well as its sensitivity to anisotropic motion. In principle, relaxation analyses of tightly binding ligands (e.g. $K_D < 1nM$) with high aqueous solubility could probe separately the free versus bound CSA tensors. This remains an area of future study. Presently, we are restricted to the assumption of site-invariant CSA tensors, as in previous studies of exchange-transferred cross-correlation.[7]

Perhaps the most critical assumption is that of overall isotropic tumbling of the ligand and receptor molecules. If we forego this assumption, then the variation in $P_B\eta_{xy,B}$ and $\eta_{xy,F}$ values can reflect not only internal mobility but also the different mean orientations of the CH bonds with respect an *anisotropic* molecular diffusion tensor. Similarly, $P_B\eta_{xy,B}/\eta_{xy,F}$ would reflect not just changes in internal ligand flexibility, but also changes in the diffusion tensor. In this scenario, computational methods would be required to help separate static from dynamic effects. Complementary measurements of residual dipolar couplings would also prove useful. While rotational anisotropy clearly complicates data interpretation, successful deconvolution of the static versus dynamic effects might help determine bound ligand orientations. We are currently pursuing work along these lines, and the results will be presented elsewhere.

Significance to Drug Design. The utility of cross-correlated relaxation experiments is that they can provide profiles of ligand flexibility that enable one to relate the inherent flexibility of ligands to the desirable properties of drugs. An example would be flexibility profiling during iterative optimization cycles aimed at enhancing ligand potency. Specifically, the $P_B\eta_{xy,B}$ data can reveal which parts of the ligand retain residual mobility in the bound state. Residual mobility is thought to diminish potency since it implies a reduction of the binding enthalpy, or suboptimal shape complementarity. The $P_B\eta_{xy,B}$ flexibility profile thus calls attention to those ligand sites where modifications could enhance the binding energy. For example, medicinal chemists can attach bulkier hydrophobic substituents to increase van der Waals contacts, or increase the number of hydrogen bond donors/acceptors. Following such modifications would be another flexibility profile along with standard activity assays and structure determination to evaluate the modification strategy and suggest new ones. Such iterative flexibility profiling would be well-suited for drug targets resisting standard structure determination and which rely mainly on ligand-based pharmacophore approaches. Moreover, augmenting pharmacophores with dynamic information could prove prescient when considering integral membrane proteins for which flexibility may be an important aspect of recognition. Iterative flexibility profiling can also help guide design strategies based on the linking of simpler molecular scaffolds to create more potent and specific inhibitors. The flexibility information can help rationalize the observed improvement (or lack thereof) of potency in terms of flexibility and not just structure. Since the binding free energies of fragments need not be additive,[54] methods that can interrogate the dynamical as well as structural consequences of fragment linking will be crucial.

The above scenarios are predicated on the assumption that the elimination of residual bound ligand flexibility will always improve potency. The more rigorous approach strives to match the bound and free state flexibility so as to minimize conformational entropy losses upon binding. To help realize this, $P_B\eta_{xy,B}/\eta_{xy,F}$ can map where the largest changes in flexibility occur. The presence of significant deviations in a $P_B\eta_{xy,B}/\eta_{xy,F}$ profile can help identify which regions of the ligand are "entropically disadvantaged".

The conformational entropy of the bound ligand is influenced by the flexibility of the protein, which can contain an active site with both rigid and flexible regions. As postulated by Morgan et al., forcing the active site to conform to a completely rigid ligand may actually reduce potency owing to an unfavorable decrease of conformational entropy.[55] There is some evidence that rigidification can lead to suboptimal potency.[56] Additionally, the need for "broad-spectrum" inhibitors against proteins with subtly different active sites (perhaps arising from drug-resistant mutations), will require ligands that retain a limited degree of flexibility to accommodate small structural differences. In short, the ability to design "adaptive" ligands, that is ligands containing strategic regions of flexibility, may prove a powerful strategy in drug design.[57] However, to design such "adaptive" ligands, we require a predictive understanding

of the molecular basis for the binding free energy. Currently, our predictive capabilities are confounded by the difficulties of understanding the molecular basis for the binding entropy. Molecular flexibility is certainly a contributor to this entropy. While increasing numbers of NMR studies are describing residue-specific changes in *protein* flexibility and relating those changes to conformational entropy,[58–62] less attention has been paid to the corresponding ligand. However, from a pharmaceutical perspective, the ligand is certainly significant since it is the object of modification. Therefore, the methods presented here fill a void by probing changes in *ligand* flexibility and, thus, ligand conformational entropy. As such, our ^{13}C cross-correlated relaxation measurements can help define strategies to enable rational modulation of the binding entropy.

Finally, while we have focused on the bound ligand flexibility in the context of enhancing binding potency, knowledge of the free ligand flexibility will also prove useful in attempts to better delineate the molecular properties critical for bioavailability. Our current understanding of oral bioavailability at the molecular level is embodied in the empirical rule sets, such as the "Rule of 5" developed by Lipinski et al.[63] Such rules, based on a retrospective study of known drugs, generally assume rigid molecules. However, as pointed out by Chaturvedi and Navia, drug flexibility can be a useful feature to promote transport across membrane barriers and thus modulate oral bioavailability.[64] By having site-specific flexibility profiles of ligands, we can begin systematic studies toward investigating this possibility.

Conclusions

In summary, we have demonstrated the use of ^{13}C CSA–DD cross-correlated relaxation methods to probe the flexibility of aromatic CH bonds in ligands that are in fast exchange between the free and receptor-bound states. The methods involve measurements at natural abundance and therefore bypass the typical paucity of isotope-enriched ligands in pharmaceutical research settings. The focus on aromatic groups is consistent with their prevalence in "drug-like" molecules.

We have demonstrated these methods on a receptor–ligand system consisting of the 42 kDa kinase domain of the p38 MAP kinase and one of its ligands, 2-phenoxybenzoic acid. Our investigations suggest that, for ligands in fast exchange between the free and receptor-bound states, transverse CSA–DD cross-correlated relaxation parameters are sensitive to the bound state relaxation properties and, hence, the bound state flexibility. For the system studied here, they have proved to be more sensitive than more standard R_1 measurements. Under certain assumptions, we can estimate the scaled bound state relaxation rate constant $P_B\eta_{xy,B}$, which provides a flexibility profile of the bound ligand. Additionally, the ratio $P_B\eta_{xy,B}/\eta_{xy,F}$ enables a comparison of flexibility changes at different ligand sites as a consequence of receptor binding. The data suggest that there is some residual

(54) Dill, K. A. *J. Biol. Chem.* **1997**, *272*, 701–704.
(55) Morgan, B. P.; Holland, D. R.; Matthews, B. W.; Bartlett, P. A. *J. Am. Chem. Soc.* **1994**, *116*, 3251–3260.
(56) Weber, P. C.; Pantoliano, M. W.; Simons, D. M.; Salemme, F. R. *J. Am. Chem. Soc.* **1994**, *116*, 2717–2724.
(57) Freire, E. *Nat. Biotechnol.* **2002**, *20*, 15–16.
(58) Akke, M.; Brüschweiler, R.; Palmer, A. G., III. *J. Am. Chem. Soc.* **1993**, *115*, 9832–9833.
(59) Yang, D.; Kay, L. E. *J. Mol. Biol.* **1996**, *263*, 369–382.
(60) Bracken, C.; Carr, P. A.; Cavanagh, J.; Palmer, A. G., III. *J. Mol. Biol.* **1999**, *285*, 2133–2146.
(61) Zidek, L.; Novotny, M. V.; Stone, M. J. *Nat. Struct. Biol.* **1999**, *6*, 1118–1121.
(62) Lee, A. S.; Kinnear, S. A.; Wand, A. J. *Nat. Struct. Biol.* **2000**, *7*, 72–77.
(63) Lipinski, C. A.; Lombardo, F.; Dominy, B. W.; Feeney, P. J. *Adv. Drug Delivery* **1997**, *23*, 3–25.
(64) Navia, M. A.; Chaturvedi, P. R. *Drug Discovery Today* **1996**, *1*, 179–189.

mobility in the protein active site and that the CH bonds undergo different extents of rigidification. Further interpretation awaits further experiments.

The relaxation methods described above can clearly be extended to tighter binding ligands (K_D < nM). For these ligands, one would require perdeuteration of the protein target to permit selective observation of the natural abundance ^{13}C signals of the ligand. Perdeuteration would also help enhance the sensitivity of the experiment by reducing relaxation losses attributed to ^{1}H$-^1$H DD interactions. Of course, the concentration of ligand would be that of the protein receptor, and therefore, receptor concentrations in excess of those described here (50 μM) would be needed.

The main limiting feature of the experiments is sensitivity. The present measurements were carried out on a conventional probe at 18.8 T. Because the ligand concentration was only 1 mM for the receptor-containing sample, we required lengthy acquisition times. One should consider, however, that cryogenic probes now exist for magnets at 18.8 T, and that these technologies will continue to become more accessible. As such, we are optimistic that natural abundance ^{13}C relaxation methods will continue to prove useful as high-field and high-sensitivity probes become more commonplace.

A more complete interpretation of the data requires not only more measurements but also deeper considerations of how to identify and cope with slower chemical exchange rates and the possibility of high rotational anisotropy. We are currently pursuing research along these lines. Nevertheless, we are encouraged by our results thus far, which suggest that cross-correlated measurements can provide molecular flexibility signatures for ligands. Such signatures, when used in concert with iterative drug design strategies (elaboration, diversification, extension, etc.), will help deepen our understanding between molecular dynamics and biological activity.

Supporting Information Available: Expressions for exchange-averaged transverse auto-relaxation rates $R^{\alpha/\beta}_{2,\mathrm{av}}$ used to simulate $\eta_{xy,\mathrm{av}}$ versus k_{off} in Figure 2. Expressions are from the Hahn−Maxwell−McConnell,[17−19] Swift−Connick,[21] and Carver−Richards [23,24] treatments of two-state chemical exchange (PDF). This material is available free of charge via the Internet at http://pubs.acs.org.

JA030154P